NASA Technical Memorandum 100714

The Seasonal Cycle of Energetics From the GLAS/UMD Climate GCM.

David M. Straus and J. Shukla

December 1988

NASA Technical Memorandum 100714

The Seasonal Cycle of Energetics From the GLAS/UMD Climate GCM

David M. Straus
Goddard Space Flight Center
Greenbelt, Maryland

J. Shukla
University Of Maryland
College Park, Maryland

National Aeronautics and
Space Administration

**Information Management
Division**

1988

Preface

The annual cycle of atmospheric energetics from a two-year integration of the GLAS/UMD Climate GCM is computed and compared to results from the European Centre analyses of the GWE year, and to previously published results on a global basis. All calculations are done in the mixed space-time domain. The main conclusions are:(i) The seasonal cycle of total eddy kinetic energy (in both hemispheres), and of the transient eddy available potential energy and the potential-to-kinetic energy conversions (mean and eddy) in the Northern Hemisphere are well simulated by the GCM. (ii) The GCM's tendency to have anomalously large mean u-winds at upper levels in high latitudes leads to excessive wintertime values of mean kinetic and available potential energies, and causes distortions in the GCM latitude-height distribution of kinetic energy and of many of the conversions. (iii) The eddy conversion of available potential to kinetic energy obtained from the GWE analyses is too weak in the upper levels, reflecting problems with the ageostrophic wind in these analyses. (iv) The conversions in the Southern Hemisphere are not well simulated by the GCM, although the observations are somewhat questionable.

1. Introduction

The periodic response of the atmosphere to the annual cycle of solar insolation constitutes a highly significant climate fluctuation. Understanding the structure of this periodic climate change (the seasonal cycle) is clearly worthwhile in itself. It should also give us insights into the more general problem of (nonperiodic) climate fluctuations. The seasonal cycle further provides an important test for General Circulation Models (GCMs), which are a widely used tool for simulating (predicting) climate change on a variety of time scales.

The purpose of this memorandum is to compare the seasonal cycle of atmospheric energetics as simulated by the GLAS/UMD Climate GCM with observations on a global basis. Since the pioneering work of Peixoto and Oort (1974) and Oort and Peixoto (1974) drew attention to the importance of the seasonal cycle of energetics, relatively little follow-up work has been done. Peixoto and Corte-Real (1982,1983) extended the calculation of the energetics to the Southern Hemisphere, but their computational procedure obscured much of the seasonal cycle. Global results for the seasonal cycle of energetics were presented in brief form by Chen and Buja (1983) and by Oort and Peixoto (1983).

The GLAS/UMD Climate GCM is briefly described by Straus and Shukla (1988a, 1988b) and is described in more detail by Randall (1982). The resolution of the GCM is four degrees in latitude by five degrees in longitude, with nine (sigma) levels in the vertical. A full complement of physical parameterizations (radiation, cumulus and large scale condensation, mountains, etc.) is included. The seasonal cycle of the mean fields, stationary waves and transient fluctuations from the two-year integration is presented in the papers of Straus and Shukla.

The GCM integration was started from initial conditions valid for November 15, 1978. During the course of the integration (which lasted slightly more than two years), the boundary conditions were prescribed to vary in a smooth seasonal cycle. The period analyzed in this memorandum is the two years extending from December 1, 1978, through November 30, 1980.

We compare the seasonal cycle of energetics from the GCM with those we have calculated using analyses of the European Centre for Medium Range Weather Forecasts (ECMWF) for the year of the Global Weather Experiment (GWE: Dec. 1, 1978 through Nov. 30, 1979). The results of Chen and Buja, who used the same data, could not be used directly for comparison, as is explained in Section 2. Results for the global energetics during the GWE were also presented by Kung and Tanaka (1983, 1984), but only for the two so-called Special Observing Periods: Jan. 1 through Mar. 5, 1979, and Apr. 30 through July 7, 1979. The earlier observational results of Peixoto and Oort (1974) and Oort and Peixoto (1974) are also used for comparison.

The scheme used to calculate the energetics, as well as details concerning both the model simulated and observed data, are given in Section 2 (also see the Appendix). Section 3 describes the seasonal cycle of the hemispherically integrated forms of energy and their conversion, generation and dissipation and gives latitude-height sections for January and July for the Northern Hemisphere. Section 4 shows the seasonal cycle of integrated energies and conversions for the Southern Hemisphere, and gives the latitude-height sections for winter and summer seasons. A summary is presented in Section 5.

2. Methods and Data

The atmospheric energy cycle as conceived by Lorenz (1955) provides a convenient framework for describing the differences in the structure of the eddies and the mean flow between the observations and the GCM. The Lorenz scheme is not the only possible one, however. There has been some very recent discussion in the literature of a formulation of energetics that treats the interactions between the eddies and the mean flow in a manner quite different from the traditional approach of Lorenz. Both Plumb (1983) and Kanzawa (1984) discuss energetics schemes based on alternate forms of the mean zonal momentum and thermodynamic equations that utilize the generalized Eliassen-Palm flux (Andrews and McIntyre, 1976, 1978; Edmon et al., 1980). These alternative forms of the equations are purported to give a conceptually clearer picture of the interactions between the eddies and the mean flow. Unfortunately, no substantial observational studies have been carried out using this new form of energetics.

While the availability of previous observational work argues for using the traditional formulation of Lorenz for the current purpose of model validation, some comments on the value of the newly proposed scheme are germane. The strength of the transformed equations is that they correctly indicate no interaction between eddies and mean flow when the eddies consist of steady, conservative waves. However, there is no general statement that can be made about the interpretative value of the transformed equations when the wave mean flow interaction is not small. Indeed, Pfeffer (1987) has shown that the observed tropospheric eddy-mean flow interaction is more easily understood in terms of the traditional form of the zonal mean momentum and thermodynamic equations than in terms of the transformed equations. (Put another way, the observed eddy-induced mean zonal flow acceleration in the troposphere is much closer to the divergence of eddy momentum flux than it is to the convergence of the Eliassen-Palm flux.) Furthermore, Plumb (1983) has argued against placing absolute significance on individual energy conversion or flux terms within any scheme. Each term is meaningful only within the context of its own particular scheme. The spirit of the discussion of energetics in this paper is consistent with these cautions; we do not infer any causal relationships on the basis of the energetics alone, but only seek to compare integrated measures of the eddy and mean-flow structures in the GCM with those in nature, with particular emphasis on the seasonal cycle.

The specific formulation of the energetics within the the overall Lorenz scheme used here is that of Peixoto and Oort (1974, hereafter referred to as PO), in which time averages of all energies and conversions are taken over a specified averaging period, with the separation between stationary (time-mean) and transient contributions being made. (PO refer to this formulation as being in the mixed space-time domain, following the terminology of Oort, 1964.) One compelling reason for choosing the mixed space-time formulation of PO is the wealth of previous work on the observed seasonal cycle of energetics in precisely this form.

PO and Oort and Peixoto (1974, referred to as OP) computed the seasonal cycle of energetics in the Northern Hemisphere from an objective analysis scheme based on five years of station data, while Peixoto and Corte-Real (1982, 1983, collectively referred to as PC) detailed the Southern Hemisphere seasonal cycle of energetics based on data from the International Geophysical Year (IGY). In addition, Oort and Peixoto (1983, referred to as OP83) gave some information on the seasonal variation of energetics in both hemispheres using the ten-year global dataset of Oort (1983). To this list we add the seasonal cycle of energetics for both hemispheres for the entire GWE year (December 1978 through November 1979) calculated in this paper from the ECMWF III-b analyses (Bengtsson et al., 1982).

Because of the substantial difference in the amount of data available for the two hemispheres, and in keeping with previous work, we carried out the calculations separately for the two hemispheres, for both the GWE and GCM data. In particular, the basic mean zonal hemispheric static stability was averaged separately over each hemisphere. Our calculations of the GWE year energetics can thus be distinguished from those of Chen and Buja (1983), who used only one global static stability and worked within the so-called space domain (Oort, 1964), in which all energies and conversions are computed separately for each day. For the GCM, the results presented (whether for a basic averaging period of a month or a season) represent the average of the two corresponding months (or seasons) from the two-year simulation. Readers should refer to PO for all pertinent details of the formulation of the basic forms of energy, their generation and dissipation, boundary fluxes,and the forms of energy conversion. In the appendix, we briefly describe the notation used in this memorandum, as well as the exact computational domain of the various calculations.

3. Northern Hemisphere Energetics

(a) Time series of integrated quantities

The annual march of the various Northern Hemisphere energy integrals is depicted in Figures 1 and 2. One month was used as the basic averaging time. The results of our calculations using the GWE data are given by the solid lines, the GCM results by the dashed lines, and the results of OP by the dotted lines.

The mean available potential energy P_M shows a very strong seasonal cycle in which the first harmonic (annual cycle) is almost as strong as the annual mean. That the GCM P_M is too large in winter is due to the presence of excessively low temperatures at upper levels over the winter pole, a problem that occurs in many GCMs. As detailed in Straus and Shukla (1988a and 1988b, hereafter referred to as SS88), excessively low temperatures are predicted

by the GCM at upper levels in high latitudes during all seasons. In winter, however, the cold anomaly is deeper than in other seasons. Correspondingly, the mean u-wind fails to decrease (as observed) above 200 millibars (mb) in any season, but the size of the upper level anomaly in the u-wind is much greater in winter than in any other season. Since the summer values are close to the observed, the simulated seasonal cycle in P_M is too strong.

The seasonal variation of the eddy available potential energy P_E is much smaller than that of P_M. It is also less clearly dominated by the annual harmonic. This holds true for both the stationary P_{SE} and the transient P_{TE} contributions. The GCM fails to capture the basic seasonal cycle in P_E beause of the second simulated maximum in summer, when the observations show a minimum. This maximum is due to the behavior of the stationary eddies (monthly mean waves) in the temperature field, which are too vigorous in the GCM in summer (see SS88). As a result, the second harmonic (semiannual cycle) in the GCM dominates the first harmonic (annual cycle). The problem is seen to occur only in P_{SE}, for although the simulated P_{TE} is consistently higher than either observed curve in Figure 1 (due to the overly vigorous model transient temperature eddies), the seasonal cycle is well simulated.

The excess pole-to-equator temperature gradient in the GCM causes excess mean zonal winds in winter, a failure reflected in the annual march of K_M shown in Figure 2. The discrepancy between the simulated and observed seasonal cycle in K_M is larger than the corresponding discrepancy in P_M, consistent with the thermal wind relationship. The simulated seasonal cycle of K_E, shown in Figure 2, agrees very well with the observations of OP and PO, but shows slightly less seasonal dependence than the GWE results. The GCM results do show a hint of a secondary maximum in summer in total K_E that is due to the anomalous behavior of the summer stationary eddies (K_{SE}). The simulated transient eddies (K_{TE}) behave rather well in terms of their overall strength.

Passing now to the integrals measuring the conversion of one form of energy to another, we see in Figure 3 a very strong seasonal cycle $C(P_M, P_E)$ in both sets of observations, with the first harmonic nearly as strong as the annual mean. Again the GCM seasonal cycle is too strong, but now the simulated results are greater than the observed throughout the year. This behavior is also manifested in the transient energy conversion $C(P_M, P_{TE})$, while the seasonal cycle of the stationary eddy conversion is more realistic.

The simulated conversion $C(P_E, K_E)$ shows a much noisier behavior than the GWE results, as seen in Figure 4. (Note that OP and PO give only the stationary eddy conversion, $C(P_{SE}, K_{SE})$). Whether this is due to excessive temporal variations on the part of the GCM or excessively smooth behavior in the ECMWF analyses is not clear. This conversion depends upon the divergent component of the wind field, which may not be handled well in the ECMWF analyses. The GCM results do give approximately the correct winter-to-summer difference, however. This is also true of the transient eddy conversion $C(P_{TE}, K_{TE})$, although here the GCM curve lies consistently below the observations. The one feature that the three curves for $C(P_{SE}, K_{SE})$ have in common is the lack of a discernible annual harmonic. The GCM's seasonal cycle runs parallel to that given by OP but is too large in magnitude, while the GWE curve is consistently flatter than the others.

The difficulty the GCM has in simulating the mean upper tropospheric jet extends to the associated kinetic energy conversion $C(K_E, K_M)$, as shown in Figure 5. While the two sets of observations yield at least the same sign, the GCM results are relatively strong and of the opposite sign. This behavior clearly stems from the transient eddies.

The conversion of mean energy $C(P_M, K_M)$, shown in Figure 4, involves the zonal mean (ageostrophic) v-wind in the formulation of OP. Because of the inability of the ECMWF analysis scheme to correctly handle this quantity, the GCM results in Figure 4 should be compared only to those of OP. We see that the observed tendency to have positive values in the winter and negative values in the summer is well captured by the GCM, although the simulated wintertime values are far too small.

The generation terms are given in Figure 6. Here the GCM results are compared to three independent estimates of OP: the solid curve was obtained by combining estimates of radiational cooling and heating due to precipitation and boundary layer processes, the dot-dashed curve results when the diabatic heating is estimated as a residual in the thermodynamic equation, while the dotted line was obtained by OP as a residual directly from the equation for the rate of change of P_M. All three agree that there is a fall maximum and a late winter minimum in G_M. This is only partly in accord with the GCM results which suggest a (weak) summer minimum and a fall maximum. The two large dots represent the results of an earlier version of the GCM (Stone, et al. , 1977). The excessively large winter values of the GCM can be attributed to the unrealistically large pole-to-equator temperature gradient, since the

generation of P_M involves not only the mean diabatic heating but also the mean temperature field.

The GCM annual march of the generation of eddy available potential energy shows a weak loss in winter and a gain in summer.

(b) Latitude-height sections

The distribution of the various forms of energy and their conversions in the latitude-height plane is indicated for January and July in the Northern Hemisphere in Figures 7 and 8 for the GWE data, and in Figures 9 and 10 for the GCM. The total energy (or conversion) is obtained from any of these distributions by multiplying by cosine(latitude) before integration over latitude and pressure.

The mean available potential energy P_M in Figure 7 is observed to have high latitude maxima near the ground and near 400 mb, and is also large in the tropics. It is small in midlatitudes, where the temperature is near its horizontal average. The conversion $C(P_M, P_E)$ is large throughout midlatitudes, reaching peak values at 700 mb and (further north) in the lower stratosphere. It tends to be dominated by the conversion to the transient eddies $C(P_M, P_{TE})$. The GWE distributions given here differ from the corresponding distribution shown in OP in that the latter show a maximum near the ground and smaller stratospheric values. P_E is distibuted similarly, although the low level maximum is now at the ground and is shifted somewhat polewards. The conversion $C(P_E, K_E)$ is confined to 850 mb and below and is large throughout the extratropics. The contributions of both stationary and transient eddies have similar patterns, with the latter being stronger in magnitude. The distribution of $C(P_{SE}, K_{SE})$ thus differs greatly from that shown by OP, which is dominated by a dipole-like pattern near 300mb. This may indicate a problem with the divergent velocity components in the ECMWF analyses, as mentioned earlier. In complete contrast to the low-level pattern of $C(P_E, K_E)$, the eddy kinetic energy itself is largest at the upper levels, with a midlatitude maximum primarily due to the transient eddies and a subtropical maximum due to the (weaker) stationary eddies. The appearance of kinetic energy at upper levels, far removed from the low-level baroclinic sources, is due to the upward propagation of wave action (Edmon et al. , 1980).

The observed barotropic conversion $C(K_E, K_M)$ shows a dipole-like structure with positive values south of the jet core and negative values to the north. In this respect it is similar to the pattern shown by OP, although the additional positive maximum at 60 degrees North (N) in the GWE data is new. The conversion $C(P_M, K_M)$ involves the zonal mean divergent v-wind, which is extremely weak in the ECMWF analyses. Hence we have shown the results of OP in Figures 7 and 8. At upper levels a dipole pattern is seen, with the negative (indirect) Ferrel cell contribution outweighing the positive (Hadley) cell part.

The summer circulation of the Northern Hemisphere is considerably less vigorous than its winter counterpart, as witnessed by the lower values of the energies and their conversions. The July distribution of P_M now shows an additional upper level maximum in the lower stratosphere, in agreement with PO. Tropical values are much less than in January, indicating a flatter temperature field. The conversion $C(P_M, P_E)$ has become negative at upper levels, while the low-level maximum of January has moved to higher latitudes near the ground in July, in addition to becoming much weaker. In contrast to the January results, this maximum is now due entirely to the transient eddies. The July distribution of P_E is similar to that of PO in the upper levels, except that in the GWE results the 300 mb maximum does not extend as far polewards as in PO. The maximum near the ground seen in January is still present in July in the ECMWF (but not in the PO) observations.

The distributions of the conversion $C(P_E, K_E)$ and of K_E itself do not change drastically from January to July, and this remains true of the transient eddy contributions. The stationary eddy component shows equatorward movement of the important features. The conversion $C(K_E, K_M)$ is again dipole-like in July, with the zero line near the latitude of the mean jet. Now, however, the negative branch of the dipole is very weak, as is the maximum at 60 N. The results for $C(K_E, K_M)$ and for K_M agree with those of OP and PO except for the appearance in the GWE data of a maximum in the subtropical stratosphere due to easterlies in this region.

Turning now to the latitude-height distribution of GCM Northern Hemisphere energetics for January (shown in Figure 9), we see that the distribution of P_M is realistic, even though its hemispheric integral is too large. In contrast, the conversion $C(P_M, P_E)$ is not well simulated by the GCM. The midtropospheric peak in the GCM (which is both too large and too high) is due mostly to the transient eddies, while the upper tropospheric structure and

anomalous secondary low-level peak are due primarily to the stationary eddies. The simulated P_E is more realistic, with a broad surface maximum which, in fact, is stronger than is observed. The lower stratospheric peak in the observations is replaced by an upper tropospheric maximum near 45 N, where the conversion $C(P_M, P_E)$ peaks.

The GCM's conversion $C(P_E, K_E)$ has the lower-level magnitude of the GWE observations, although it peaks at 850 mb, not at the ground. The GCM pattern also shows a great deal of upper tropospheric structure, with a broad dipole pattern at 300 mb and a second one near the model top. The 300 mb dipole pattern (as well as the low-level maximum) is dominated by the transient eddies, the upper-level one, by the stationary eddies.

The GCM simulation of the eddy kinetic energy K_E reaches a peak near the model top, in sharp contrast to the (GWE) observed 250 mb peak. It seems likely that this is a manifestation of the temporal and longitudinal variations of the anomalously large upper-level jet in the model. This feature also seems to be associated with an erroneous kinetic energy conversion $C(K_E, K_M)$. Although the observed dipole (with zero line near the mean jet) is well reproduced, its vertical structure is not. It is noteworthy that the cause of the error in the sign of the hemispheric integral of $C(K_E, K_M)$ is apparently not the anomalous vertical structure of the conversion, but an error in the relative strengths (and extents) of the two dipole components. The GCM distribution of K_M both confirms that the simulated mean jet is ten degrees too far poleward, as well as demonstrating its failure to close above 150 mb. The simulated mean conversion $C(P_M, K_M)$ shows clearly the observed contributions from the Hadley and Ferrel cells.

We have already seen that the July Northern Hemispheric integrals of P_M and of $C(P_M, P_E)$ from the GCM were more realistic than the January values. The improvement in simulation during summer is also evident in the latitude-height distributions, seen in Figure 10. The conversion shows a high latitude maximum near the ground (dominated by transient eddies), with an upper-level region of negative conversion overlying one of the opposite sign. The July distribution of P_E is also realistic in the GCM; broad maxima appear in the upper troposphere (although they are too intense and not high enough) and near the ground. The overly strong subtropical peak at upper levels in the GCM is due to the excess vigor of the stationary waves.

The evaluation of the July pattern of $C(P_E, K_E)$ is not straightforward, for again the GWE distribution does not resemble that of OP (not shown) for the stationary eddies. (The results of OP show a dipole centered at 100 mb at 30 N and small low-level values.) The low-level GCM center in the tropics is due to the stationary eddies and appears to be erroneous.

The fidelity of the simulated July pattern of K_E (compared to the GCM's failure in January due to excessive activity near the model top) supports the notion that the January problem is related to the mean jet, for in July the mean GCM jet is less anomalous, although it again does not close at upper levels (see SS88).

The greater realism of the GCM July mean jet is also reflected in the simulation of the conversion $C(K_E, K_M)$, whose magnitude decreases correctly in the upper troposphere. (Note also the more realistic total hemispheric integral for July in Figure 5.) Here it is the stationary eddy contribution that is the more realistic, the GCM's pattern of $C(K_{SE}, K_M)$ strongly resembling the observed stationary pattern, which in turn is very similar to the total shown in Figure 10. (The simulated stationary conversion does have an unrealistic positive peak near 300 mb in the tropics, however.)

The simulated pattern of K_M shows more negative shear above the jet core in July than was evident in January, but the shear is still not negative enough. Excessive upper-level westerlies at high latitudes and a deficiency of upper-level tropical easterlies are noted. The patterns of $C(P_M, K_M)$ given by OP and by the GCM are in qualitative agreement, indicating the dominance of the Ferrel cell contribution over that of the Hadley cell.

4. Southern Hemisphere Energetics

(a) Time series of integrated quantities

Although the observational database is much poorer for the Southern than for the Northern Hemisphere, estimates of the Southern Hemisphere energetics have been published recently. PC calculated the energy cycle from IGY data, whereas Oort and Peixoto (1983, referred to as OP83) used a ten-year global homogeneous dataset (Oort, 1983) to compute the energetics of the Southern Hemisphere. Both of these calculations employed the space-time

formulation discussed earlier. PC used two six-month seasons (Oct.-March and April-Sept.) as their basic time-averaging periods, whereas OP83 used the more conventional three-month seasons (Dec.-Feb. and June-Aug.). We here present the space-time energetics of the Southern Hemisphere calculated from the ECMWF GWE data and from the GCM. In order to detail the annual march of the energetics and yet compare with the previous observational work, we present two sets of calculations. In the first, the month was used as the basic averaging period. In the second, three-month seasons (Dec.-Feb., March-May, June-Aug., and Sept.-Nov., referred to as DJF, MAM, JJA, SON) were used. The hemispheric totals are given for both sets of calculations, while the latitude-height distributions are given for the three-month seasons only. Because the transient eddy contribution is the dominant one in most of the eddy quantities presented here, we present only the total eddy quantities. Time series of the basic energy integrals are given in Figure 11, the conversions in Figure 12, and the boundary terms and $G(P_M)$ in Figure 13.

The annual march of P_M in the GCM shows the same flaw as in the Northern Hemisphere, namely that the excessive wintertime values imply an overly vigorous seasonal cycle in the GCM. The seasonal results of OP83 lie between the GCM and GWE measures of P_M, so that the extent of the GCM overestimate of the seasonal cycle is unclear. The observed and simulated seasonal cycles of P_E show a broad maximum in winter when viewed from the month-to-month perspective, but the values of the GCM P_E are too large. Again, the seasonal observations of OP83 show a more vigorous circulation than do the GWE results. (The increase in P_E in going from the summer to the fall seasons in both the GCM and the GWE curves is due to the change of the structure of the zonally averaged, monthly mean temperatures from one month to the next, as these changes are considered part of the transient eddy contribution in the seasonal calculations).

The GCM's winter polar night jet problem is reflected in K_M, which for winter is twice that of the GWE observations. The summer values are also too large, but since K_M is relatively small then, the GCM's annual harmonic appears to be much too strong. The discrepancy between the two sets of observational results is almost as strong as between the GWE results and those of the GCM. The values of OP83 are smaller in summer (DJF) because the jet in the data used by OP83 is weaker; in winter (JJA) the analysis of OP83 shows no signs of the stratospheric polar night jet that is present at 100 mb and 60 South (S) in the GWE results. In marked contrast to K_M, the simulation of K_E seems quite realistic with regard to its anuual variations. Both observational datasets and the GCM indicate slightly higher values in winter than in summer.

The conversion of potential energy from mean to eddy $C(P_M, P_E)$ is far too strong in the GCM Southern Hemisphere, although the month-to-month changes are fairly realistic. (In other words, the annual harmonic is reasonable but the annual mean is too large.) Note that the winter and summer seasonal values of OP83 are smaller than the GWE values. The GCM conversion $C(P_E, K_E)$ is only moderately weaker than is observed from April through November, but is significantly too small from December through March, giving the GCM's conversion an unrealistically large annual harmonic.

In interpreting the curves for the mean potential to kinetic energy conversion $C(P_M, K_M)$, we must keep in mind the limitations of the ECMWF analyses with regard to the zonal mean (ageostrophic) v-wind. The seasonal results for the GCM and the analysis of OP83 indicate a reasonable simulation in summer (DJF), while the GCM gives a slightly negative winter (JJA) value, contrasting with the positive value of OP83. The observational picture is, however, quite uncertain, for the six-month seasonal conversions given by PC are both negative: -0.81 W/m^2 for summer (Oct.-Mar.) and -0.13 W/m^2 for winter (Apr.-Sept.).

The GWE and OP83 observations show better agreement with respect to the value of the barotropic conversion $C(K_E, K_M)$, indicating a positive conversion throughout the year, and a weak seasonal cycle. As in the Northern Hemisphere, the simulated conversion is consistently of the wrong sign.

The generation of mean potential energy $G(P_M)$ for GCM, shown in Figure 13, has a distinct seasonal cycle with a summer maximum and a winter minimum. The only observational estimates available that were not obtained as residuals are given in PC (indicated in the figure by horizontal bars). These were calculated for the two six-month seasons, and are strictly speaking not comparable to the values computed with a one- or three-month averaging time. Nevertheless, the overall values seem to be in broad agreement.

(b) Latitude-height sections

The latitude-height distribution of the basic forms of energy and their conversions is

depicted in Figures 14-17. Here winter and summer refer to the three-month periods JJA and DJF respectively, so that the "transient eddy" contribution includes the time dependence of the zonal flow within each season. The three-month seasons were chosen (as opposed to single winter and summer months) partly so that the distributions of $C(P_M, K_M)$ given by PC (who used six-month seasons) could be used in place of the suspect GWE distributions without too much incompatibility.

The observed distributions during Southern Hemisphere winter (JJA) are similar to the Northern Hemisphere January results. P_M has a strong high latitude contribution and a weaker tropical one, and its conversion into P_E takes place predominantly in midlatitudes, with maxima in the stratosphere and lower troposphere. The eddy available potential energy has qualitatively similar patterns in both hemispheres, although the Southern Hemisphere has far less total energy. In contrast, the conversion $C(P_E, K_E)$ seems to be as strong in the Southern as in the Northern Hemisphere, and again is confined to the lower troposphere. The eddy kinetic energy is similarly distributed in both hemispheres, while the distribution of kinetic energy conversion shows dipoles centered near the mean tropospheric jet in both hemispheres, with the sign of the dipole corresponding to acceleration (deceleration) equatorwards (polewards) of the mean jet.

The most dramatic difference between the hemispheres seems to be the distribution of $C(P_M, K_M)$. In the January Northern Hemisphere distribution of OP, the (negative) Ferrel cell contribution dominated, followed by the (positive) Hadley cell contribution. In the six-month winter Southern Hemisphere pattern reported by PC, the polar direct cell is as important as the Ferrel cell, while the Hadley cell is less important. There is also a positive center associated with the polar night jet. The accuracy of the latitude-height distribution in both hemispheres remains questionable.

The winter-to-summer changes in many of the Southern Hemisphere patterns are remarkably similar to the corresponding Northern Hemisphere changes, but the dramatic loss of vigor in the Northern Hemisphere summer circulation is less evident in the Southern Hemisphere. The weakening of P_M in the tropics and the appearance of the high-latitude lower-stratospheric maximum that occurred in northern summer also occurs in the Southern Hemisphere, as does the winter-to-summer change in the sign of $C(P_M, P_E)$ at upper levels. Further, the summertime distributions of both P_E and K_E in the Southern Hemisphere and the conversion between them are qualitatively similar to their winter counterparts. In contrast, the conversion $C(K_E, K_M)$ shows a seasonal change: the negative center of the dipole pattern in southern winter disappears in the summer, while the positive center intensifies and moves polewards. A dramatic winter-to-summer change in K_M is noted, reflecting the disappearance of the polar night jet, giving a seasonal change that is opposite to that in the Northern Hemisphere. Also the Ferrel cell contribution to $C(P_M, P_E)$ actually strengthens in summer, again contrary to the seasonal change experienced in the Northern Hemisphere.

Turning our attention to the distribution of the GCM winter (JJA) energetics in the latitude-height plane, we see that P_M is fairly realistic, but that the mean flow to eddy conversion of available potential energy compares less favorably to the GWE observations. The GCM conversion is centered at midlevels, with large negative values at low levels, a region of large positive conversion in the observations. In addition, the observed lower stratospheric conversion is absent in the GCM results. Surprisingly, the low-level negative GCM conversion occurs in the same region as a very intense maximum of P_E, indicating a local flow of potential energy from the eddies to the zonal mean. This maximum in P_E is present in the observations also, but in the GCM it is too intense.

The GCM conversion $C(P_E, K_E)$ is strong in low levels, in agreement with the GWE observations. However, the GCM strong upper-level conversions are not in agreement with the GWE results, although the simulated dipole-like pattern implies a good deal of cancellation in the total. (Again, the accuracy of the GWE conversion remains questionable.) The eddy kinetic energy of the GCM captures the observed center at 300 mb and 50 S, but not the maximum at 30 S. The dipole-like patterns in the observed conversion $C(K_E, K_M)$ are reproduced in the GCM results, but their orientation is not realistic, possibly because of the anomalous latitude-height profile of the mean zonal wind (as witnessed by the pattern of mean kinetic energy). As in the Northern Hemisphere, the incorrect sign of the hemispheric integral of this conversion is due to relatively subtle errors in the magnitude of the two components of the dipole.

The simulated pattern of $C(P_M, K_M)$ agrees with that reported by PC in midlatitudes, where the Ferrel cell produces a broad upper level of negative conversion and a (weaker) low-level positive region, although the negative conversion lies further poleward in the GCM

results. The GCM disagrees with the PC observations in the tropics, where the GCM ascribes a much more prominent role to the Hadley cell, and at high latitudes, where it gives the polar direct cell a much weaker one.

The winter (JJA)-to-summer (DJF) shift in the GCM distribution of P_M shows a weakening in the tropics (as observed), but does not indicate the observed summer minimum near 250 mb. The simulated seasonal shift in the conversion $C(P_M, P_E)$ is not realistic, since the observationally indicated movement of the low-level maximum upward and equatorward and the appearance of negative conversions at upper levels are not simulated by the GCM, which basically leaves the dominant center at 500 mb unshifted. The simulated seasonal shift of P_E is also not particularly realistic, for the GCM's mid- and upper-level patterns show little shift in position. The level of realism with which the GCM captures the conversion $C(P_E, K_E)$ is about the same in summer as in winter, while there is a noticeable equatorward shift in the simulated upper-level maximum.

The eddy kinetic energy continues to be realistic in summer, while the poleward movement of the main dipole structure in $C(K_E, K_M)$ is well simulated. Now, however, the simulated dipole is confined to the upper levels, with the conversion negative everywhere at 500 mb, in disagreement with the observations. The poleward shift of the subtropical jet (and hence K_M) in summer is well simulated, although the observed negative shear in the lower stratosphere is not well modelled. Both the GCM and the observations indicate the dominance of the Ferrel cell contribution in the summertime mean conversion $C(P_M, K_M)$.

5. Summary

The seasonal cycle of both observed and simulated energetics is summarized in the box diagrams given in Figures 18-21. These figures, as well as the following salient points, summarize our findings.

- The seasonal cycle of the total eddy kinetic energy in both hemispheres, and of the mean conversion $C(P_M, K_M)$, the transient eddy available potential energy, and the conversion $C(P_E, K_E)$ in the Northern Hemisphere, are well simulated. The GCM distribution of these quantities in the latitude-height plane is basically realistic, although the GCM's Northern Hemisphere K_E, K_{TE}, and $C(P_M, K_M)$ show some distortion in the area of the model's (unrealistic) upper-level jet. The GWE results for $C(P_E, K_E)$ are dominated by low levels for both hemispheres and both seasons, and for stationary and transient contributions, separately. The GWE results thus contrast sharply with those given by OP for the stationary component, in which the conversion is dominated by the upper levels. The GCM conversion is generally strong at both upper and lower levels, with the Northern Hemisphere stationary pattern in broad agreement with the observations in January.

- The difficulty the GCM has with the upper-level jet is associated with the excess wintertime values of P_M and K_M in both hemispheres, although the overall pattern of the former in the latitude-height plane is realistic. In spite of the fact that the conversion $C(K_E, K_M)$ has the wrong sign throughout the year in both hemispheres, its latitude-height distribution is not unrealistic, although distortions in the region of the (GCM) upper-level jet are present.

- The stationary eddies of the GCM are not totally realistic, leading to excessive summertime values in the Northern Hemisphere contributions of P_{SE} and K_{SE}. The distribution of these quantities is realistic, with the exception of P_{SE} in northern summer and K_{SE} in northern winter, the latter being unrealistic at upper levels, perhaps due to the model jet problem. The stationary eddies in the Southern Hemisphere are rather weak, as observed.

- The GCM's Northern Hemisphere energy conversion $C(P_M, P_E)$ has an unrealistic seasonal cycle, due to excessively large wintertime values. This conversion is dominated by the transient eddies in the GCM.

- The energetic conversions of the GCM appear to be unrealistic as a whole in the Southern Hemisphere, although the accuracy of the observations is questionable.

- The dominant boundary flux term $B(P_M)$ is well simulated in the Northern Hemisphere, while the only conclusion we can draw regarding the Southern Hemisphere is that the winter GCM value has at least the right order of magnitude.
- Finally, we feel that considering the observational uncertainties in the generation and dissipation terms, it is hard for us to draw any conclusion regarding how realistically the GCM treats these source/sink terms. Note that comparison between distinct GCM's would at least determine the range of variability of generation and dissipation processes within models.

Appendix A. Notation used in energetics calculations

The energetics scheme used is precisely that given by PO and OP, with no further approximations introduced. Two salient features of this formulation are as follows: l (i) the conversion between available potential and kinetic energy is given by the inner product of the velocity vector and the gradient of geopotential height, and (ii) the "space-time" formulation is used, in which the transient component of the zonally averaged flow contributes to the "transient eddies." The notation used is as follows:

P_M = mean available potential energy
P_E = eddy available potential energy
$P_E = P_{TE} + P_{SE}$
P_{TE} = transient eddy contribution to P_E
P_{SE} = stationary eddy contribution to P_E
K_M = mean kinetic energy
K_E = eddy kinetic energy
$K_E = K_{TE} + K_{SE}$, with K_{TE}, K_{SE} defined analagously to P_{TE}, P_{SE}
$C(P_M, P_E)$ = conversion of P_M to P_E
$C(P_M, P_E) = C(P_M, P_{TE}) + C(P_M, P_{SE})$
$C(P_E, K_E)$ = conversion of P_E to K_E
$C(P_E, K_E) = C(P_{TE}, K_{TE}) + C(P_{SE}, K_{SE})$
$C(K_E, K_M)$ = conversion of K_E to K_M
$C(K_E, K_M) = C(K_{TE}, K_M) + C(K_{SE}, K_M)$
$C(P_M, K_M)$ = conversion of P_M to K_M
$G(P_M)$ = generation of P_M
$G(P_E)$ = generation of P_E
$B(P_M)$ = equatorial flux of P_M, measured positive northwards.

Appendix B. Computational Grids

The GCM data were available on a 4-degree latitude by 5-degree longitude grid at the following 11 pressure levels: 100 mb, 200 mb, 300 mb, 400 mb, 500 mb, 600 mb, 700 mb, 800 mb, 850 mb, 900 mb, and 1000 mb. The vertical integrals were taken to go from 1000 mb to 10 mb, the model top. The horizontal integrals were taken to go from 2 N (2 S) to the North (South) Pole. The boundary fluxes were computed at 2 N (2 S) for the Northern (Southern) Hemisphere.

The ECMWF GWE analysis data were interpolated to the same latitude-longitude grid used by the GCM, and were available at the following 11 pressure levels: 50 mb, 100 mb, 150 mb, 200 mb, 250 mb, 300 mb, 400 mb, 500 mb, 700 mb, 850 mb, and 1000 mb. The vertical integrals were taken to go from 1000 mb to 0 mb, while the horizontal integrals were taken exactly as for the GCM.

References

Andrews, D. G., and M. E. McIntyre, 1976: Planetary waves in horizontal and vertical shear: The generalized Eliassen-Palm relation and the mean zonal acceleration. J. Atmos. Sci., 33 , 2031-2048.

Andrews, D. G., and M. E. McIntyre, 1978: Generalized Eliassen-Palm and Charney-Drazin theorems for waves in axisymmetric flows in compressible atmosphere. J. Atmos. Sci., 35 ,175-185

Bengtsson, L, M. Kanamitsu, P. Kallberg and S. Uppala, 1982: FGGE 4-dimensional data assimilation at ECMWF. Bull. Amer. Meteor. Soc., 63 ,29-43.

Chen, T.-C., and L. C. Buja, 1983: A comparison study for the time variation of the atmospheric energetics between two hemispheres during FGGE year: Annual variation and vacillation. Proceedings of the First International Conference on Southern Hemisphere Meteorology, , Sao Jose dos Campos, Brazil. July 31-Aug. 3, 1983. American Meteorological Society, pp. 21-24.

Edmon, H. L., B. J. Hoskins and M. E. McIntyre, 1980: Eliassen-Palm cross sections for the troposphere. J. Atmos. Sci., 37 , 2600-2616.

Kanzawa, H., 1984: Quasi-geostrophic energetics based on a transformed Eulerian equation with application to wave-zonal flow interaction problems. J. Meteor. Soc. Japan, 62 , 36-51.

Kung, E. C., and H. Tanaka, 1983: Energetics analysis of the global circulation during the special observing periods of FGGE. J. Atmos. Sci., 40 , 2575-2592.

Kung, E. C., and H. Tanaka, 1984: Spectral characteristics and meridional variations of energy transformations during the first and second special observing periods of FGGE. J. Atmos. Sci., 41 , 1836-1849.

Lau, N.-C., and A. H. Oort, 1982: A comparative study of observed Northern Hemisphere circulation studies based on GFDL and NMC analyses. Part II: Transient eddy statistics and the energy cycle. Mon. Wea. Rev., 110 , 889-906.

Lorenz, E. N., 1955: Available potential energy and the maintenance of the general circulation. Tellus 7 , 157-167.

Manabe S., and J. L. Holloway, Jr., 1975: The seasonal variation of the hydrological cycle as simulated by a global model of the atmosphere. J. Geophys. Res., 80 , 1617-1649.

Oort, A. H., 1983: Global atmospheric circulation statistics, 1958-1973. NOAA Professional Paper 14, Rockville, MD, 180 pp.

Oort, A. H., 1964: On estimates of the atmospheric energy cycle. Mon. Wea. Rev., 92 , 483-493.

Oort, A. H., and J. P. Peixoto, 1974: The annual cycle of energetics of the atmosphere on a planetary scale. J. Geophys. Res., 79 , 2705-2719.

Oort, A. H., and J. P. Peixoto, 1983: Global angular momentum and energy balance requirements from observations. Adv. in Geophysics, 25.

Otto-Bliesner, B. L., G. W. Branstator and D. D. Houghton, 1982: A global low-order spectral general circulation model. Part I: Formulation and seasonal climatology. J. Atmos. Sci., 39 , 929-948.

Peixoto, J. P., and J. A. M. Corte-Real, 1982: The energetics of the general circulation of the atmosphere in the Southern Hemisphere during the IGY. Part I: The distribution of atmospheric energy. Arch. Meteor. Geophys. Biocl., A31 , 277-301.

Peixoto, J. P., and J. A. M. Corte-Real, 1983: The energetics of the general circulation of the atmosphere in the Southern Hemisphere during the IGY. Part II: The cycle of the energetics of the atmosphere in the Southern Hemisphere. Arch. Meteor. Geophys. Biocl., A32 , 1-21.

Peixoto, J. P., and A. H. Oort, 1974: The annual distribution of atmospheric energy on a planetary scale. J. Geophys. Res., 79 , 2149-2159.

Pfeffer, R. L., 1987: Comparison of conventional and transformed Eulerian diagnostics in the troposphere. Quart. Jour. Roy. Meteor. Soc., 113 , 237-354.

Plumb, R. A., 1983: A new look at the energy cycle. J. Atmos. Sci., 40 , 1669-1688.

Randall, D. A., 1982: Monthly and seasonal simulations with the GLAS Climate Model. Proc. Workshop on Intercomparison of Large-Scale Models used for Extended Range Forecasts , Reading, ECMWF, pp. 107-166

Stone, P. H., S. Chow and W. J. Quirk, 1977: The July climate and a comparison of the January and July climates simulated by the GISS model. Mon. Wea. Rev., 105 , 170-194.

Straus, D. M., and J. Shukla, 1988a: A comparison of a GCM simulation of the seasonal cycle of the atmosphere to observations. Part I: Mean fields and the annual harmonic. Atmosphere-Ocean , to be published.

Straus, D. M., and J. Shukla, 1988b: A comparison of a GCM simulation of the seasonal cycle of the atmosphere to observations. Part II: Stationary waves and transient fluctuations. Atmosphere-Ocean , to be published.

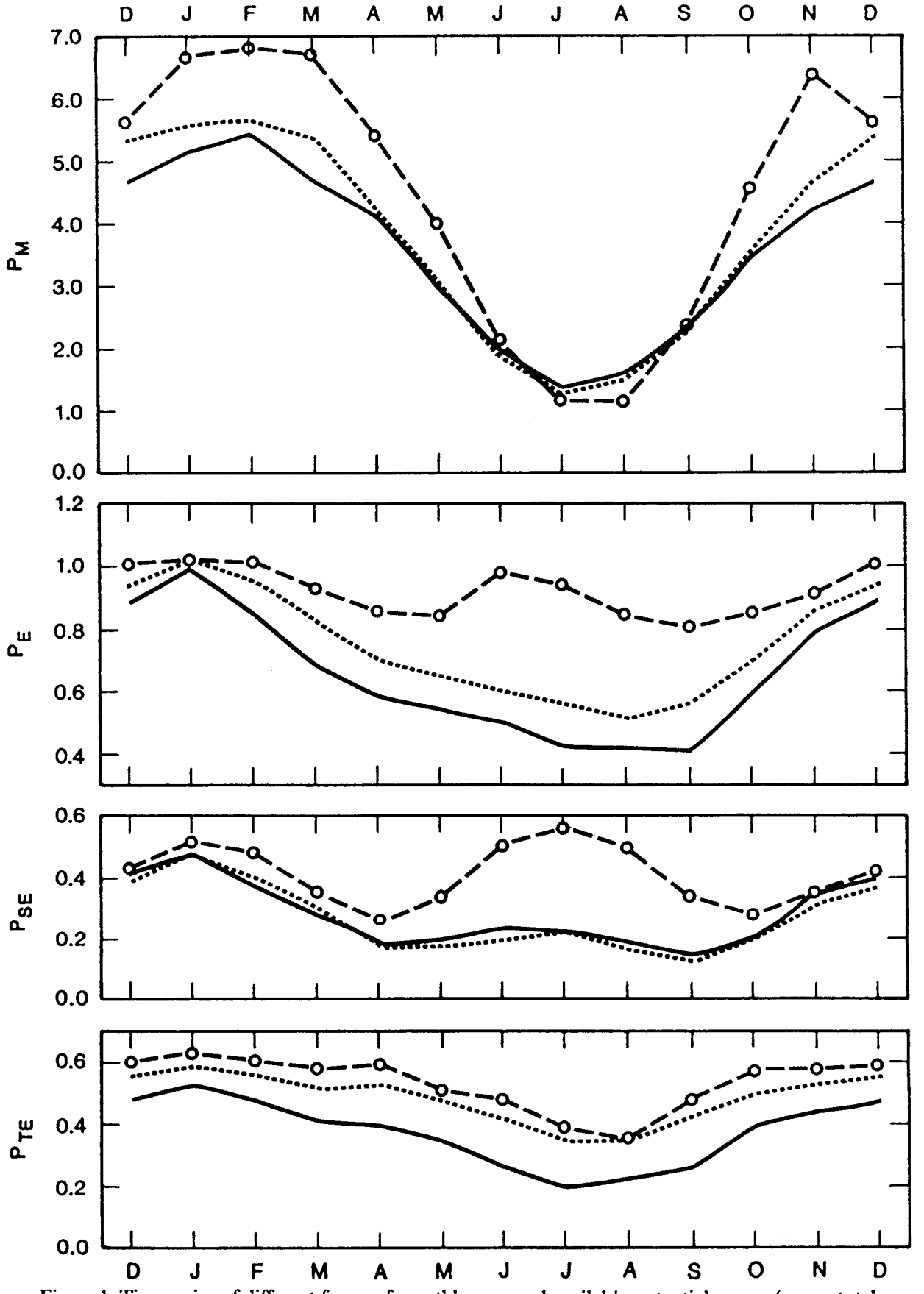

Figure 1. Time series of different forms of monthly averaged available potential energy (mean, total eddy, stationary eddy and transient eddy) averaged over the Northern Hemisphere. The solid curves are the results from the ECMWF GWE data, the dashed curves with open circles are the results from the GCM, and the dotted curves are the results of Peixoto and Oort (1974). Units are $10^6 Joule/m^2$.

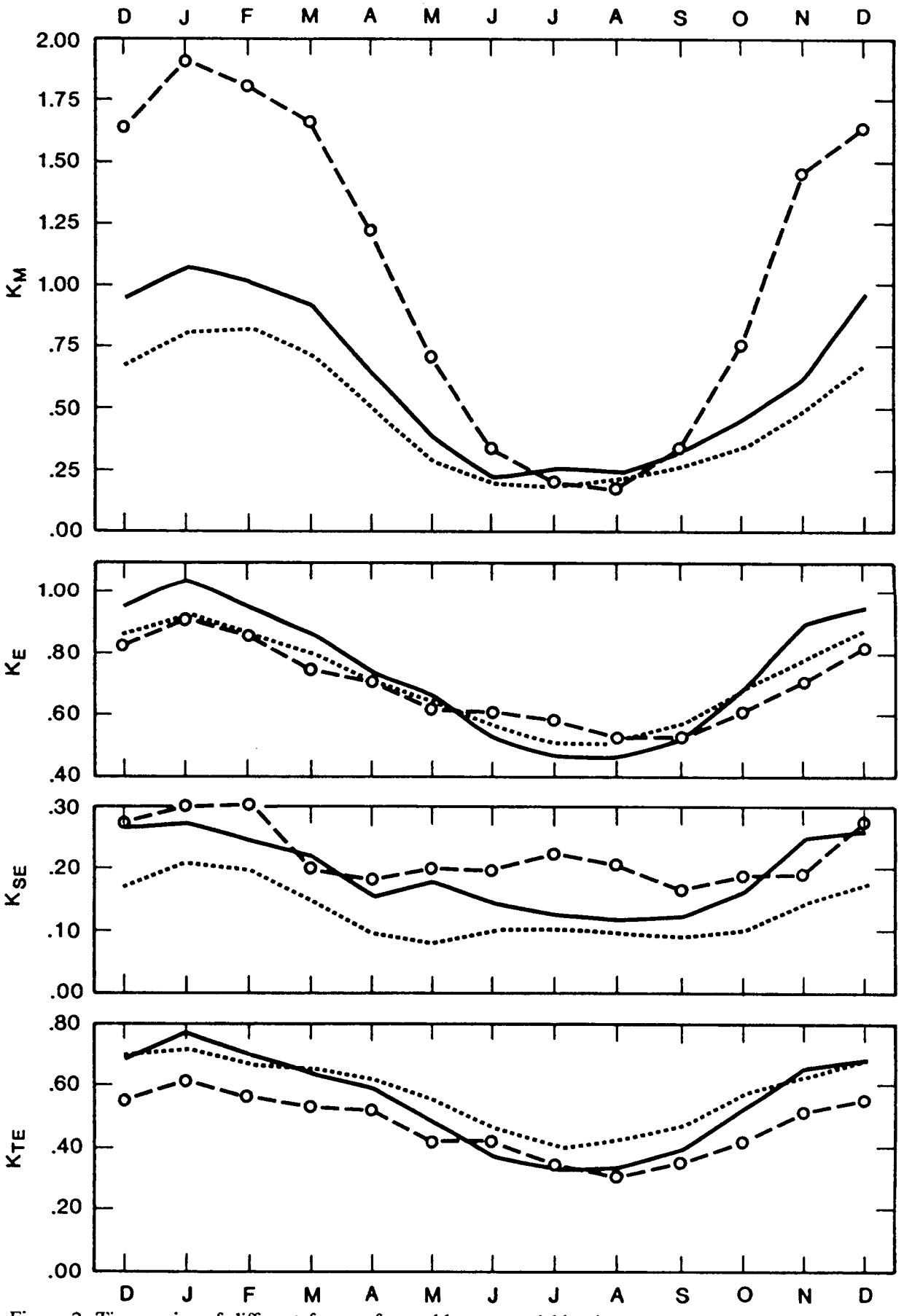

Figure 2. Time series of different forms of monthly averaged kinetic energy (mean, total eddy, stationary eddy and transient eddy) averaged over the Northern Hemisphere. Otherwise as in Figure 1. Units are $10^6 Joule/m^2$.

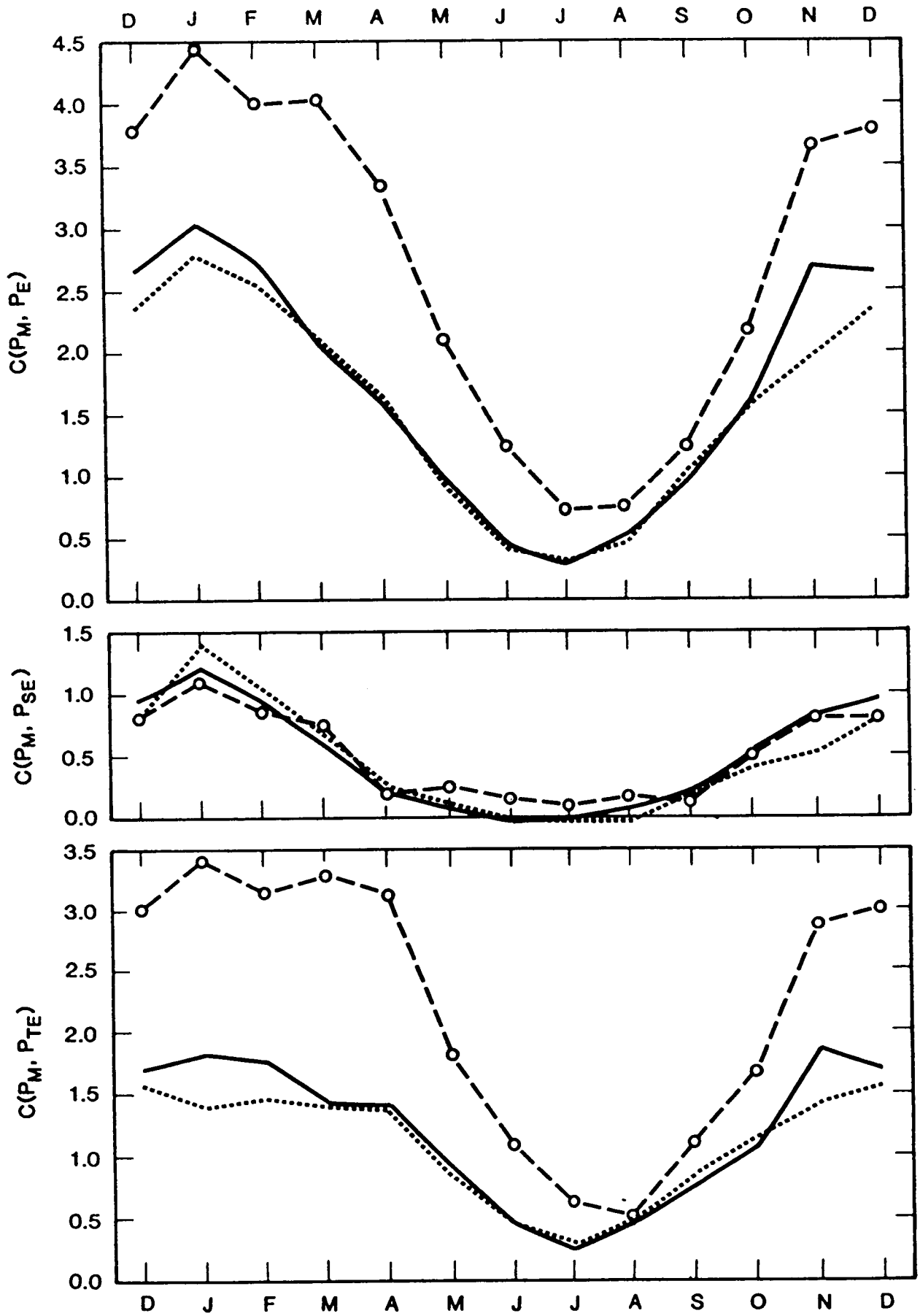

Figure 3. Time series of different forms of monthly averaged available potential energy conversions (mean-to-total eddy, mean-to-stationary eddy, and mean-to-transient eddy) averaged over the Northern Hemisphere. Otherwise as in Figure 1, except that dotted lines are taken from Oort and Peixoto (1974). Units are *Watts/m²*.

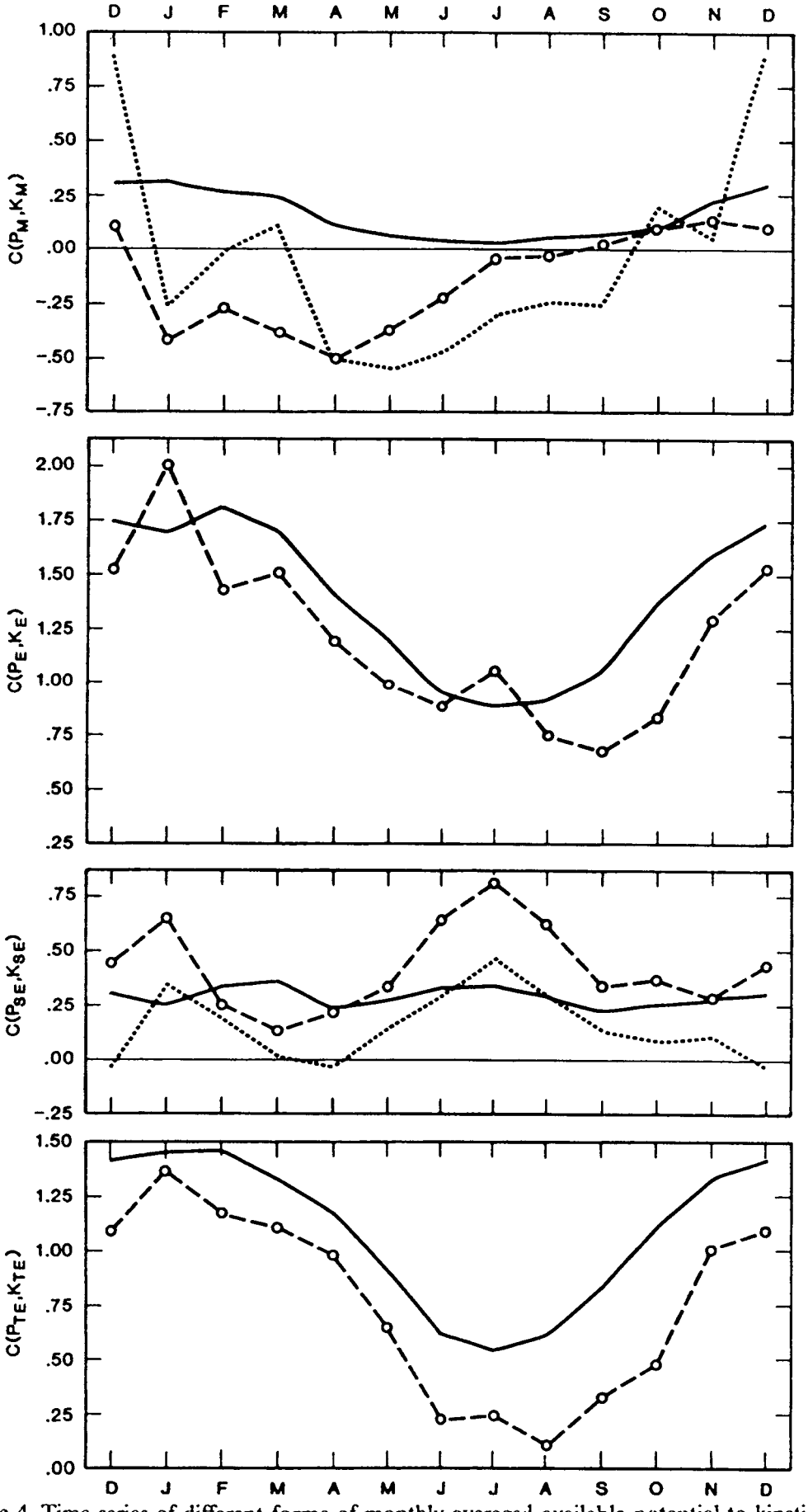

Figure 4. Time series of different forms of monthly averaged available potential-to-kinetic energy conversions (mean, total eddy, stationary eddy and transient eddy) averaged over the Northern Hemisphere. Otherwise as in Figure 3. Units are *Watts/m²*.

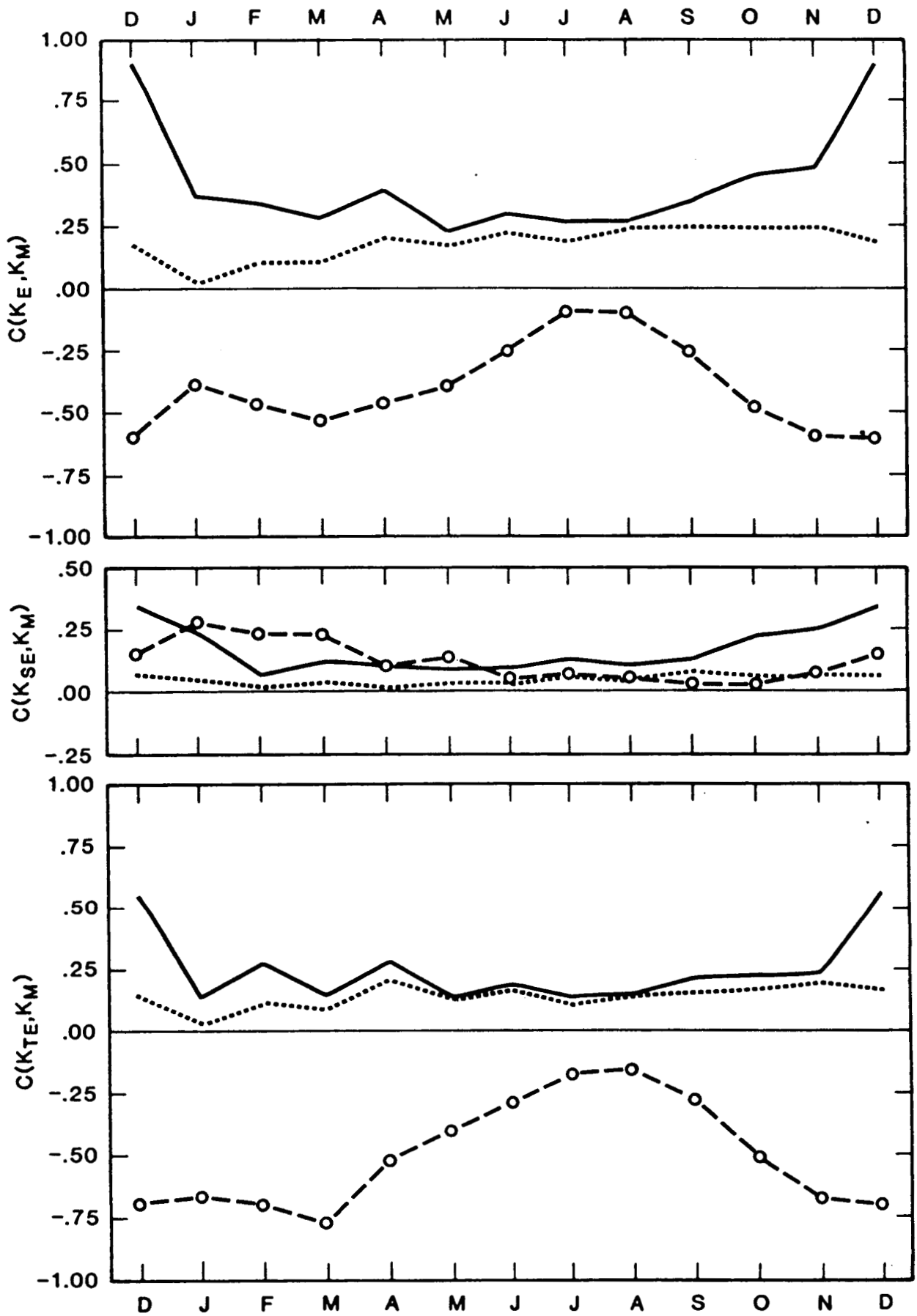

Figure 5. Time series of different forms of monthly averaged kinetic energy conversions (mean-to-total eddy, mean-to-stationary eddy and mean-to-transient eddy) averaged over the Northern Hemisphere. Otherwise as in Figure 3. Units are *Watts/m²*.

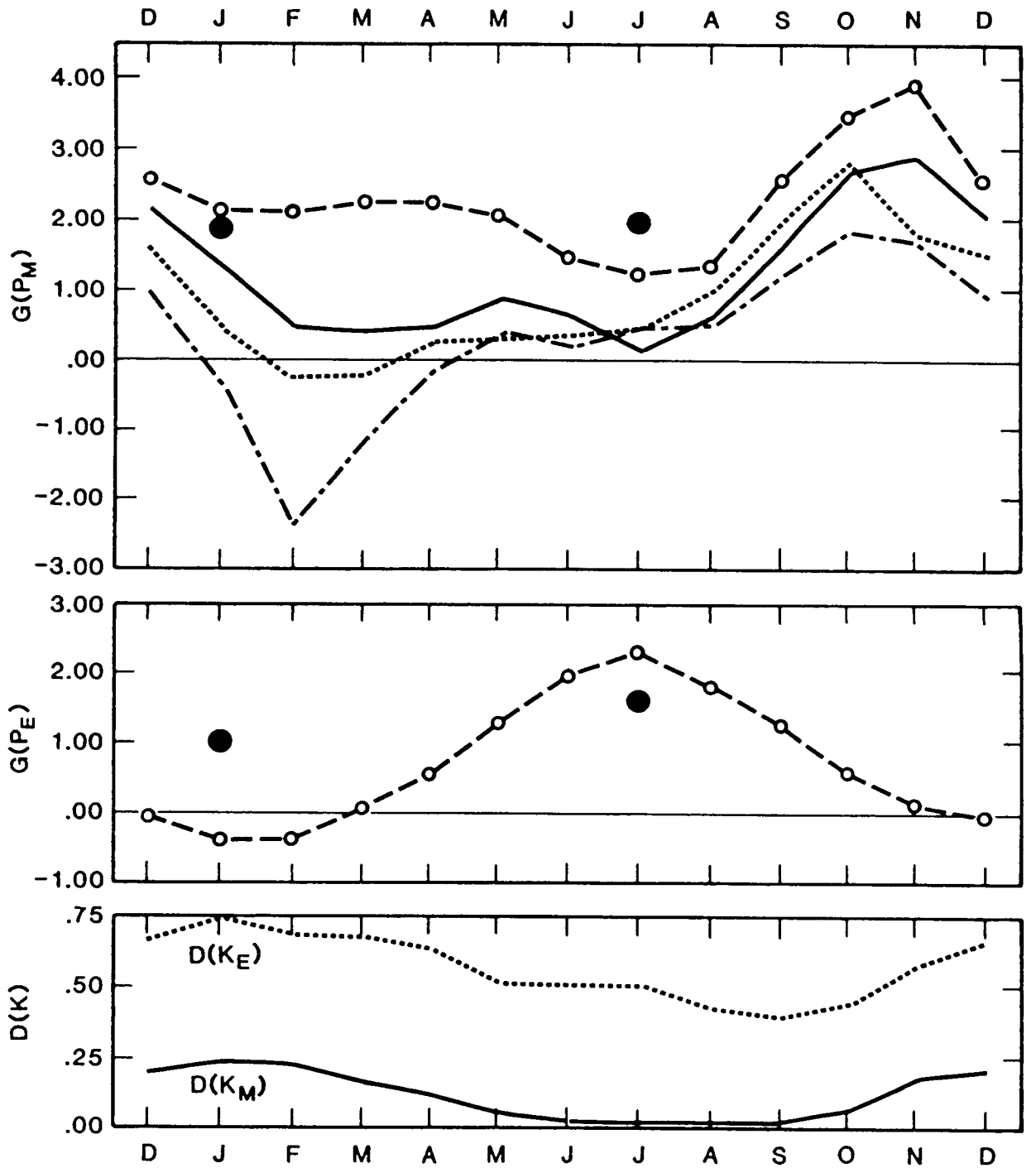

Figure 6. Time series of generation of mean and eddy available potential energy and of dissipation of mean and eddy kinetic energy, averaged over the Northern Hemisphere. In the top panels, the solid, dotted and dashed-dotted lines are estimates from Oort and Peixoto (1974, see text for details), while the dashed lines with open circles are from the GCM and the large solid dots from Stone et al., (1977). The bottom panel is the dissipation from the GCM only. Units are *Watts/m²*.

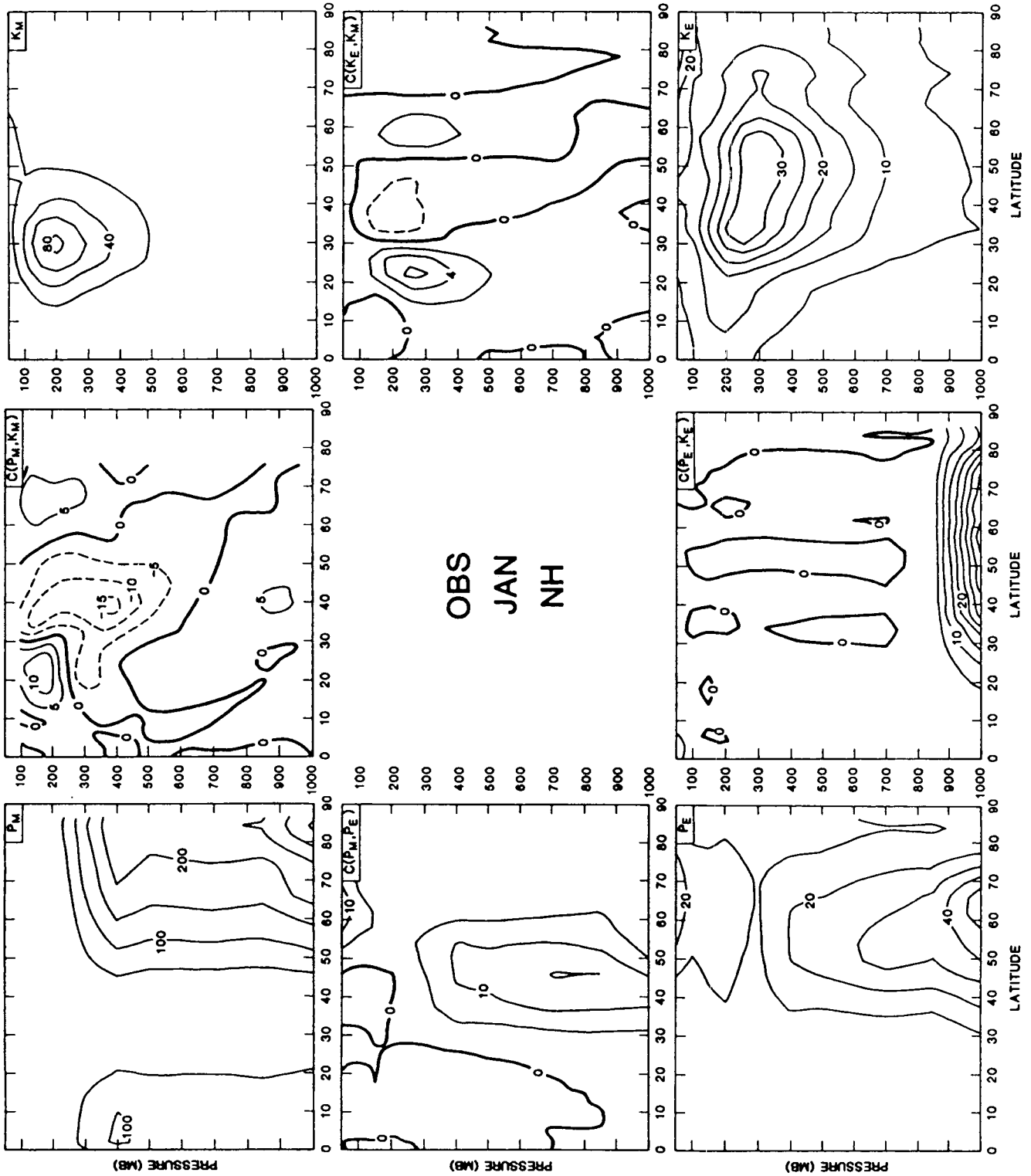

Figure 7. Latitude-pressure sections of zonally averaged energies and conversions from the ECMWF GWE analyses for January, 1979 (Northern Hemisphere). Units are $10^6 Joules/(m^2 bar)$ for energies, $Watts/(m^2 bar)$ for conversions.

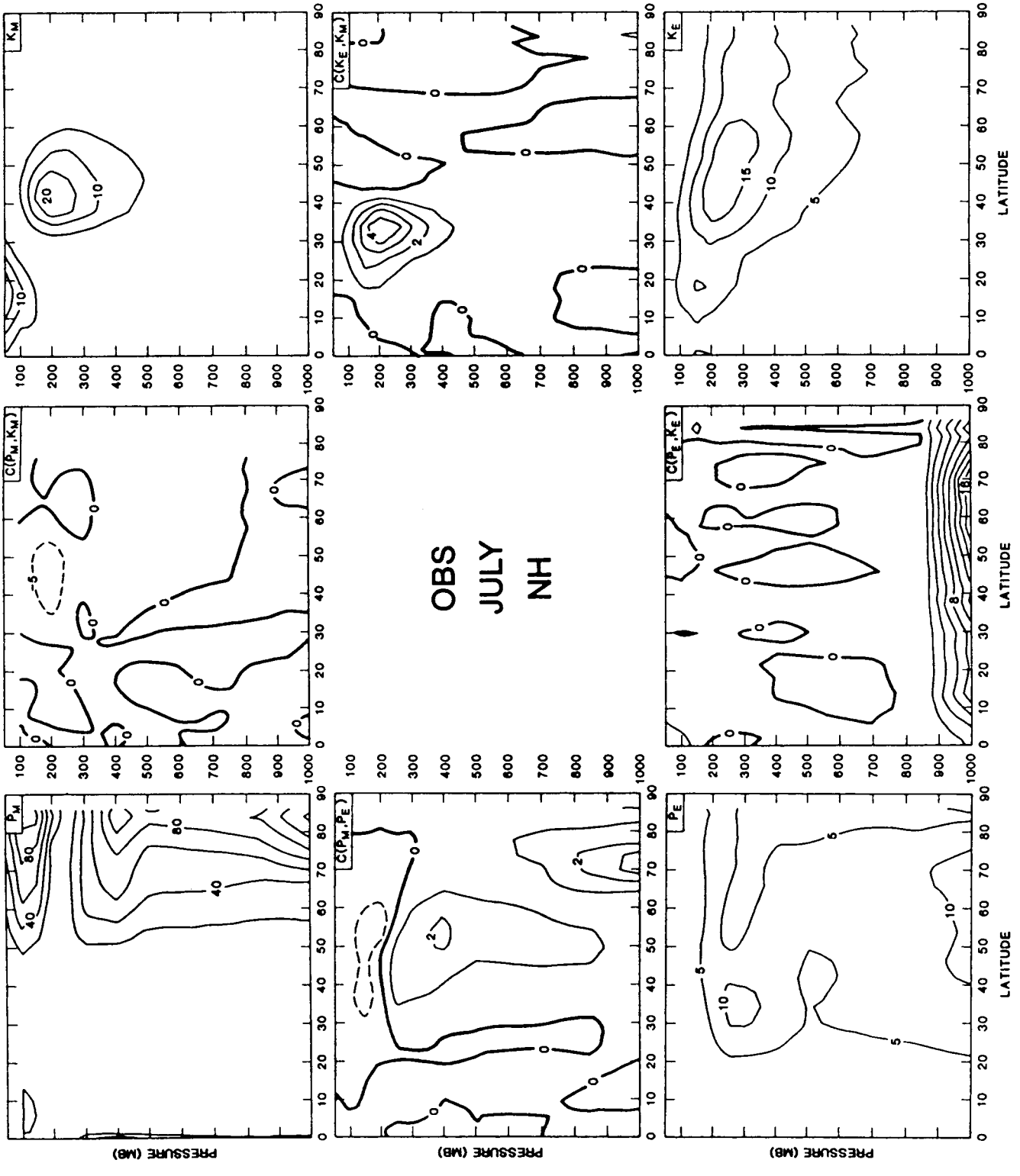

Figure 8. Latitude-pressure sections of zonally averaged energies and conversions from the ECMWF GWE analyses for July, 1979 (Northern Hemisphere). Otherwise as in Figure 7.

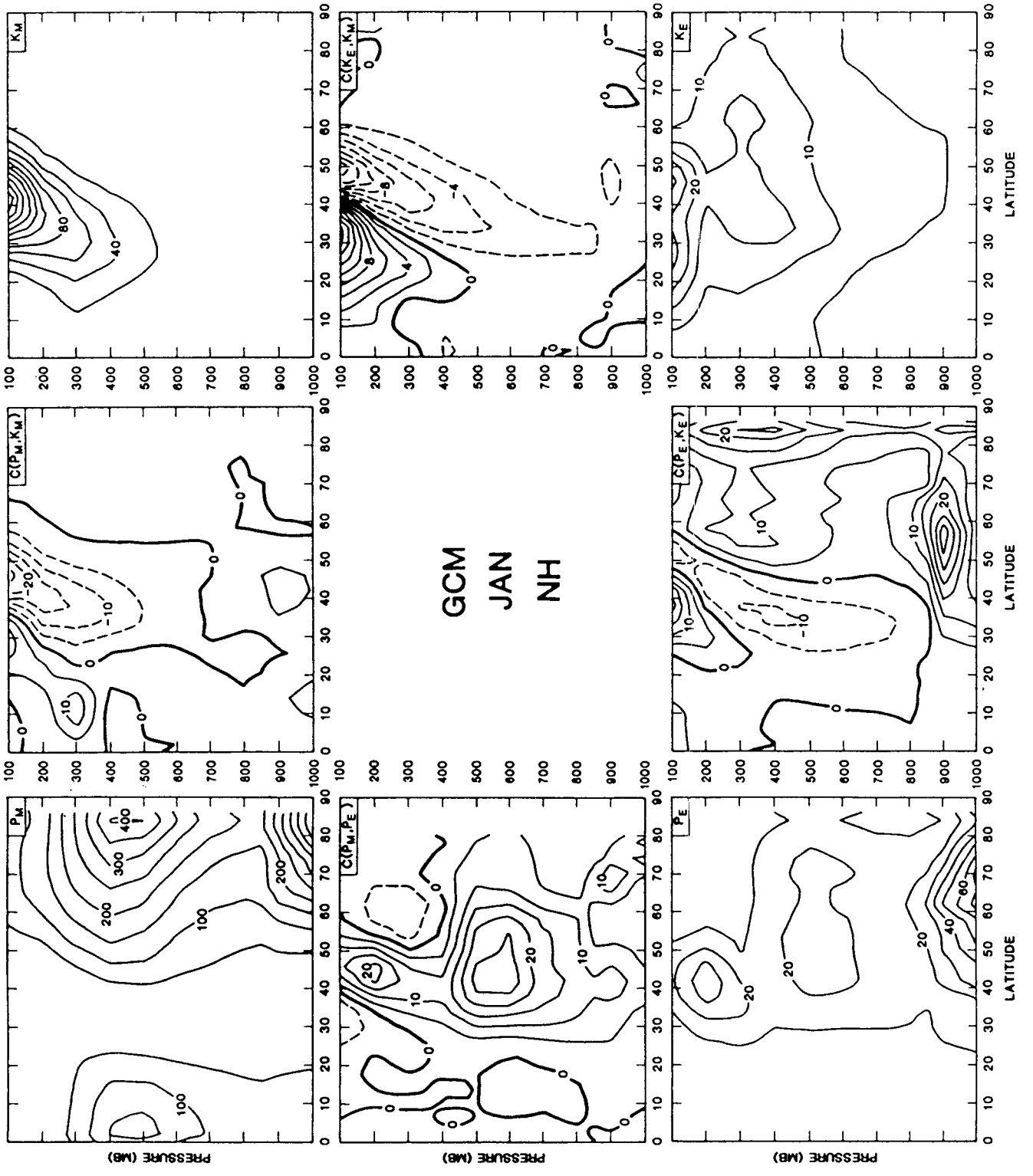

Figure 9. Latitude-pressure sections of zonally averaged energies and conversions from the GCM for January (Northern Hemisphere). Otherwise as in Figure 7.

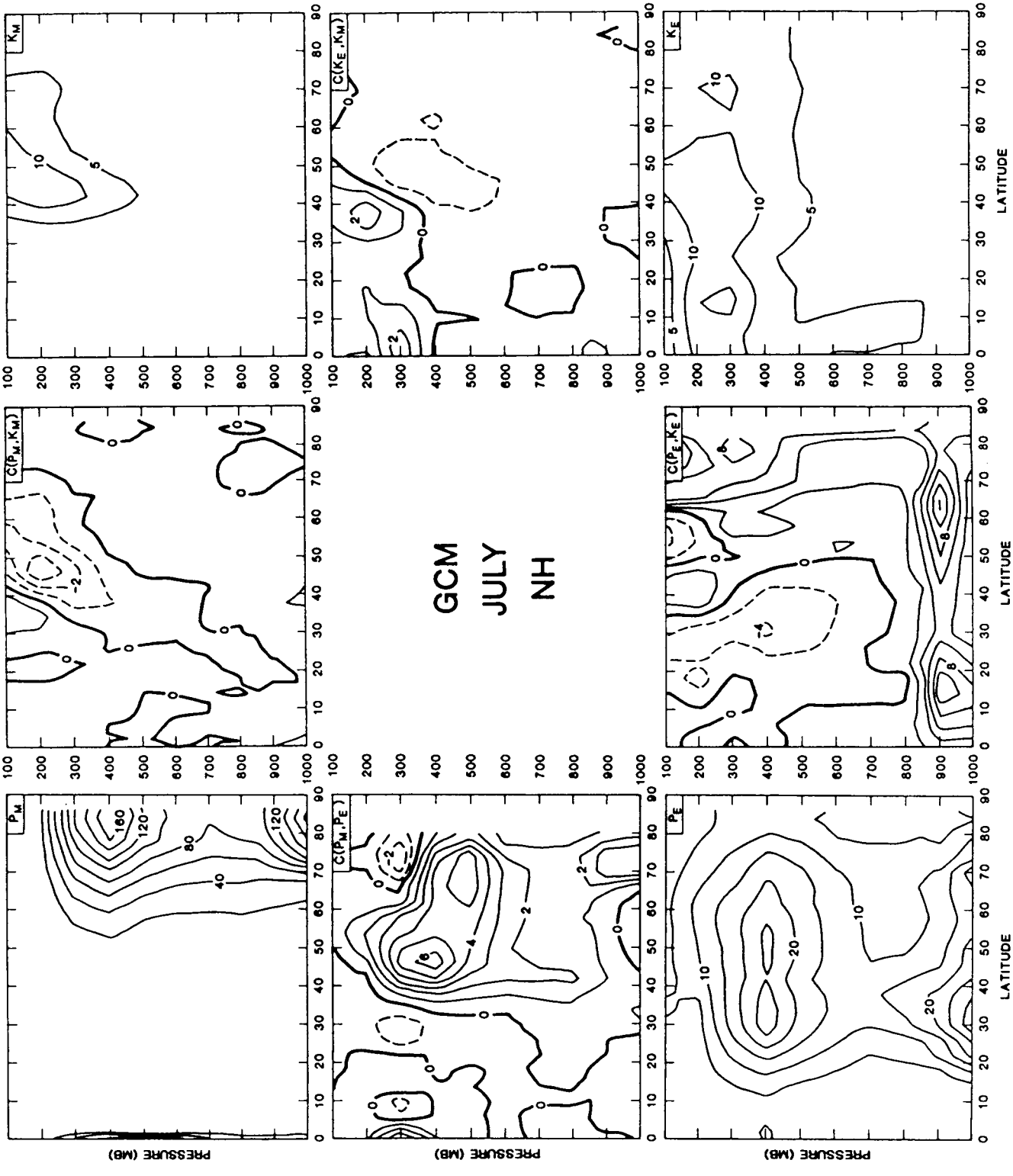

Figure 10. Latitude-pressure sections of zonally averaged energies and conversions from the GCM for July (Northern Hemisphere). Otherwise as in Figure 7.

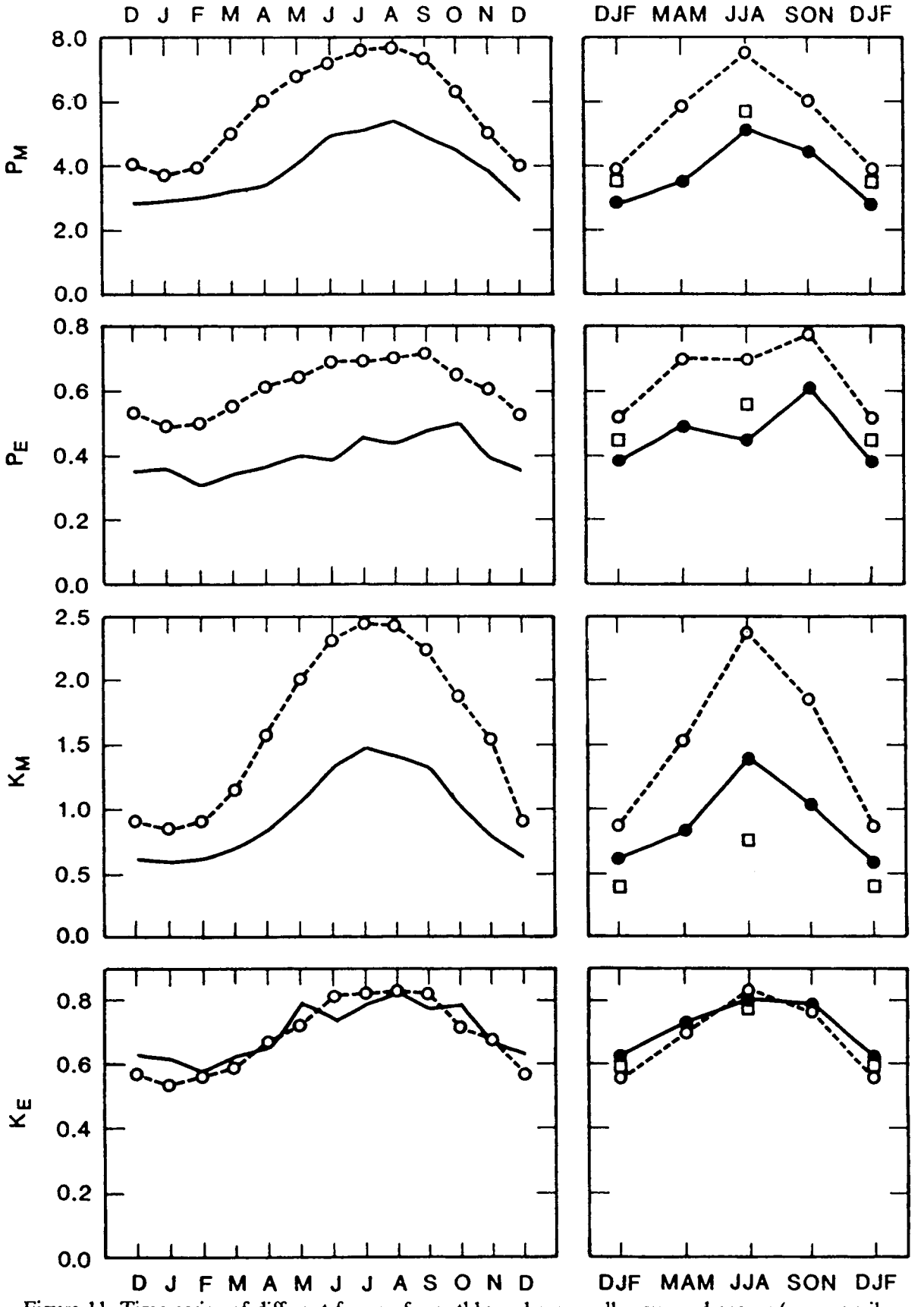

Figure 11. Time series of different forms of monthly and seasonally averaged energy (mean available potential, eddy available potential, mean kinetic and eddy kinetic) averaged over the Southern Hemisphere. Solid curves are from the ECMWF GWE analyses, dashed curves with open circles are from the GCM, and boxes are from Oort and Peixoto (1983). Units are $10^6 Joule/m^2$.

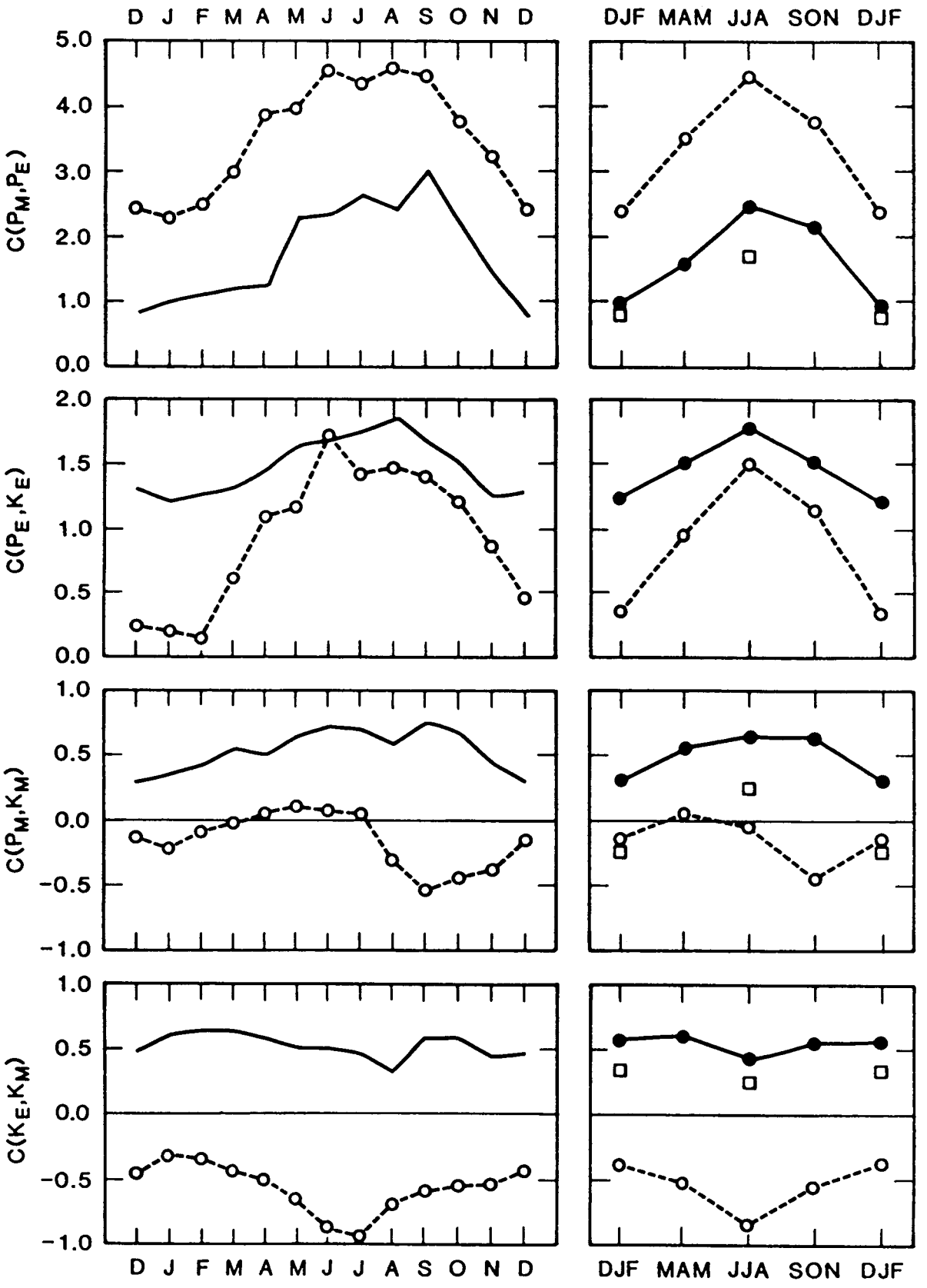

Figure 12. Time series of monthly and seasonally averaged conversions in the Southern Hemisphere. Otherwise as in Figure 11.

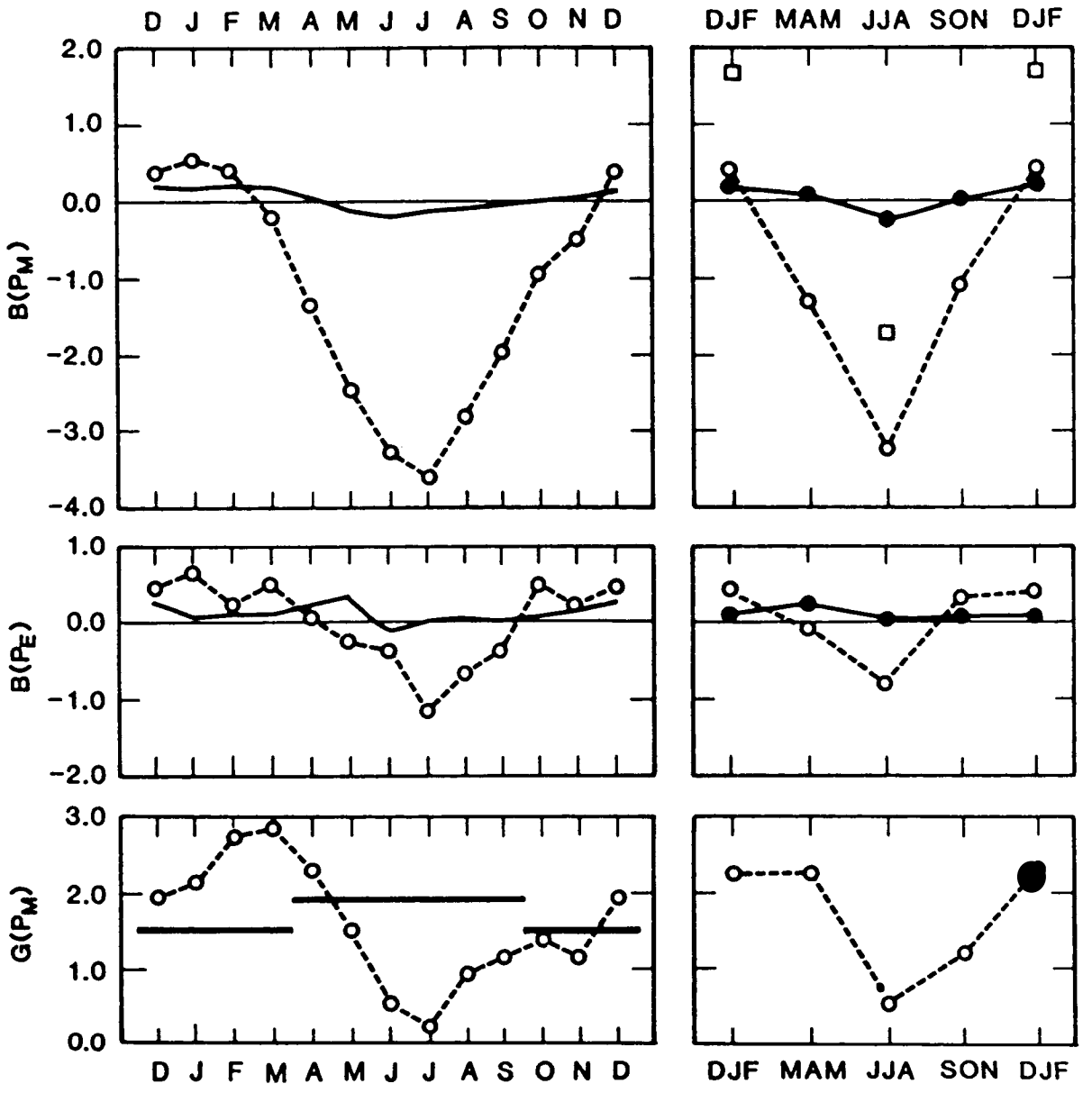

Figure 13. Time series of monthly and seasonally averaged flux of mean and eddy available potential energy northward across 2 S (top two panels), and the generation of mean available potential energy averaged over the Southern Hemisphere (bottom panel). Horizontal bars are from Peixoto and Corte-Real (1983, see text). Units are $Watts/m^2$

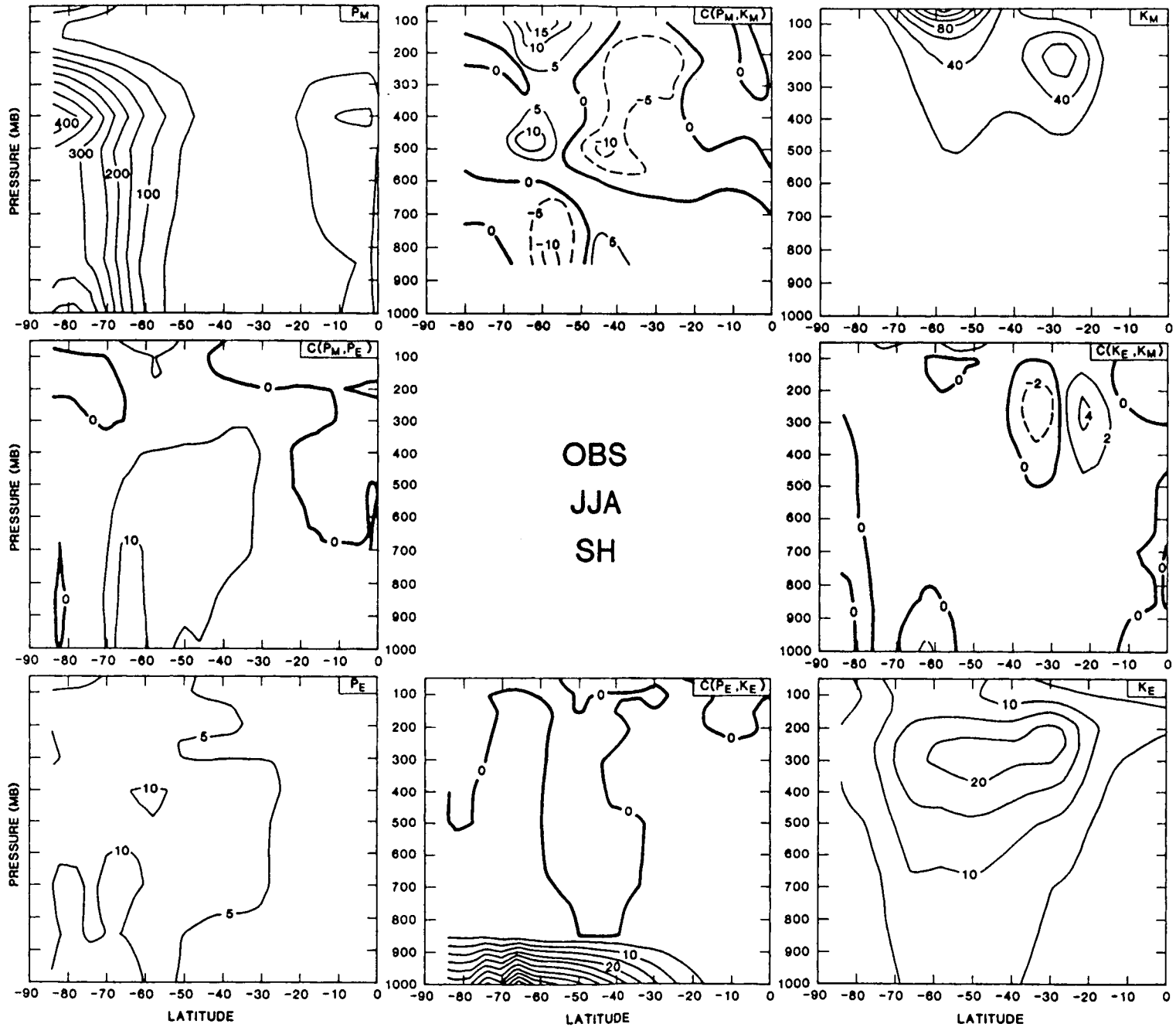

Figure 14. Latitude-pressure sections of zonally averaged energies and conversions from ECMWF GWE analyses for June-August 1979 in the Southern Hemisphere. Otherwise as in Figure 7.

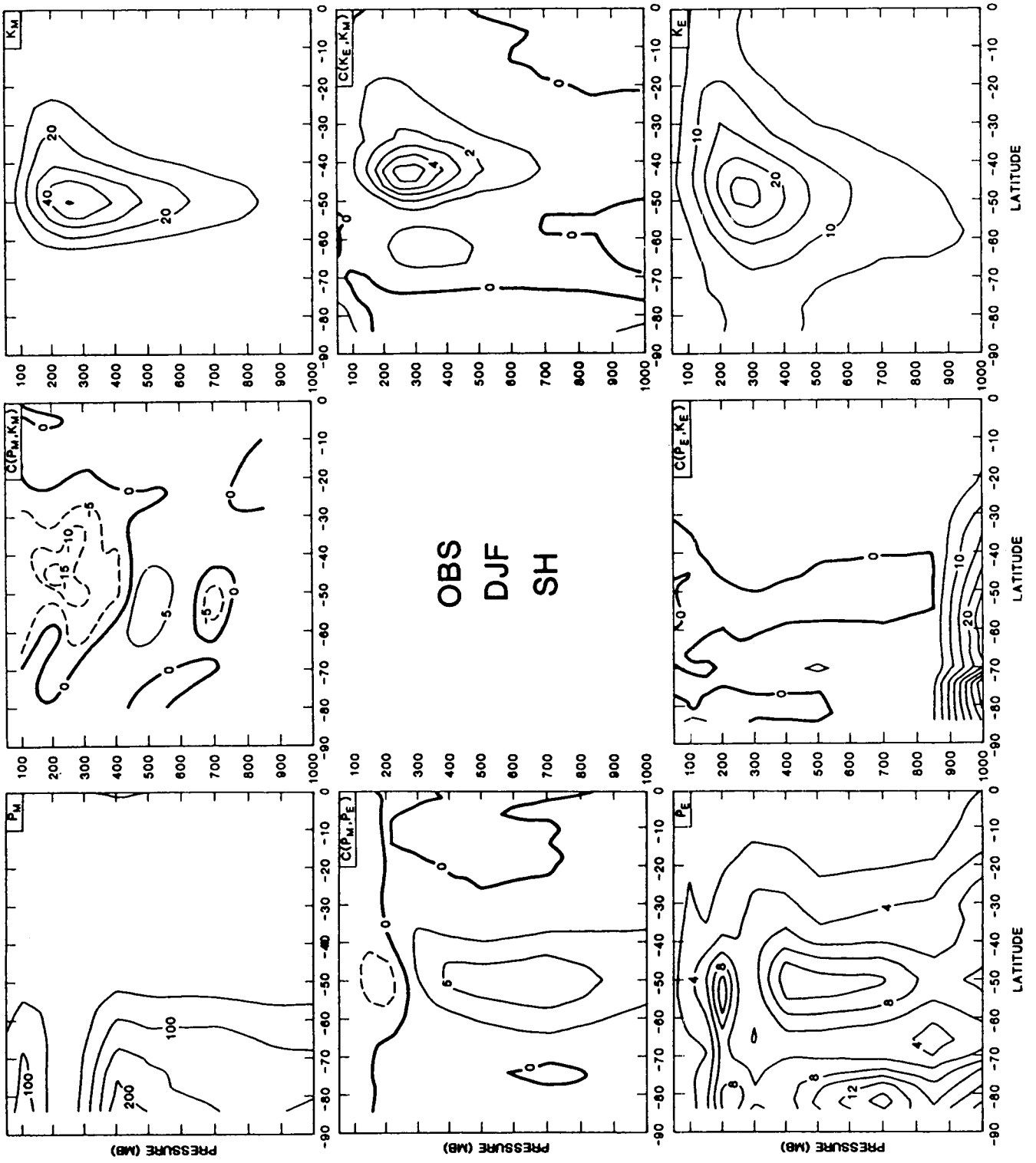

Figure 15. Latitude-pressure sections of zonally averaged energies and conversions from ECMWF GWE analyses for Dec. 1978 - Feb. 1979 in the Southern Hemisphere. Otherwise as in Figure 7.

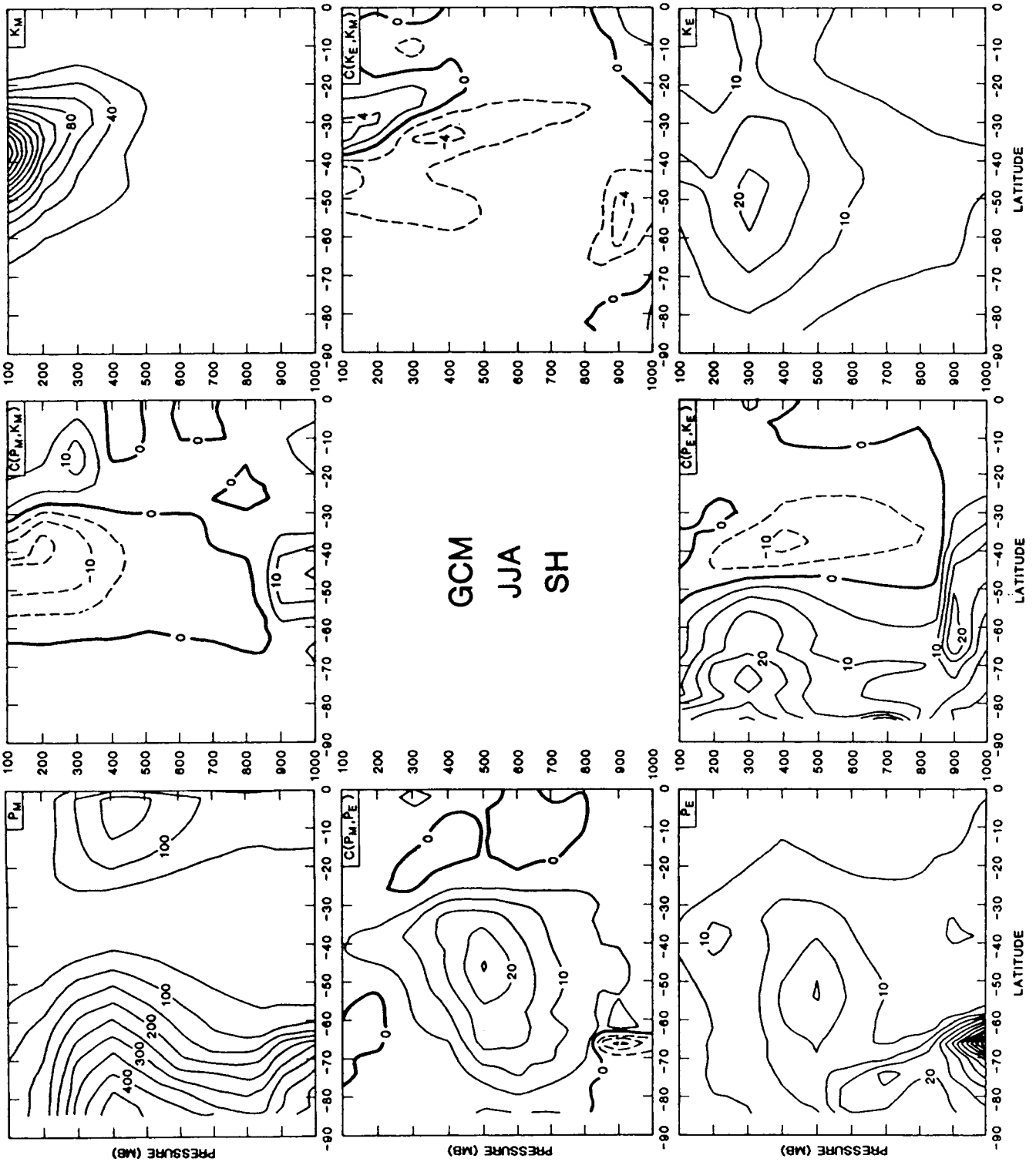

Figure 16. Latitude-pressure sections of zonally averaged energies and conversions from the GCM for June-August in the Southern Hemisphere. Otherwise as in Figure 7.

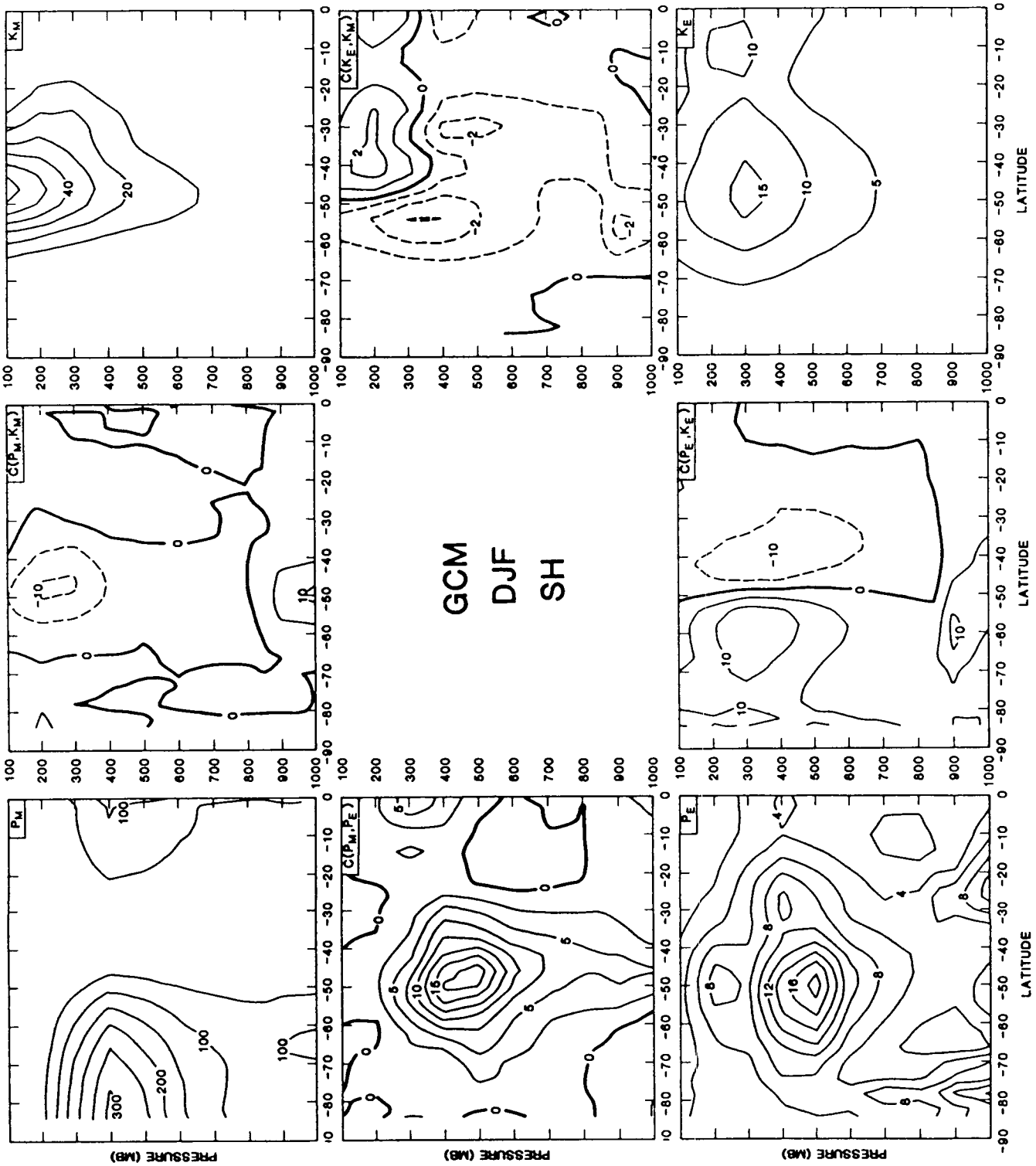

Figure 17. Latitude-pressure sections of zonally averaged energies and conversions from the GCM for Dec.- Feb. in the Southern Hemisphere. Otherwise as in Figure 7.

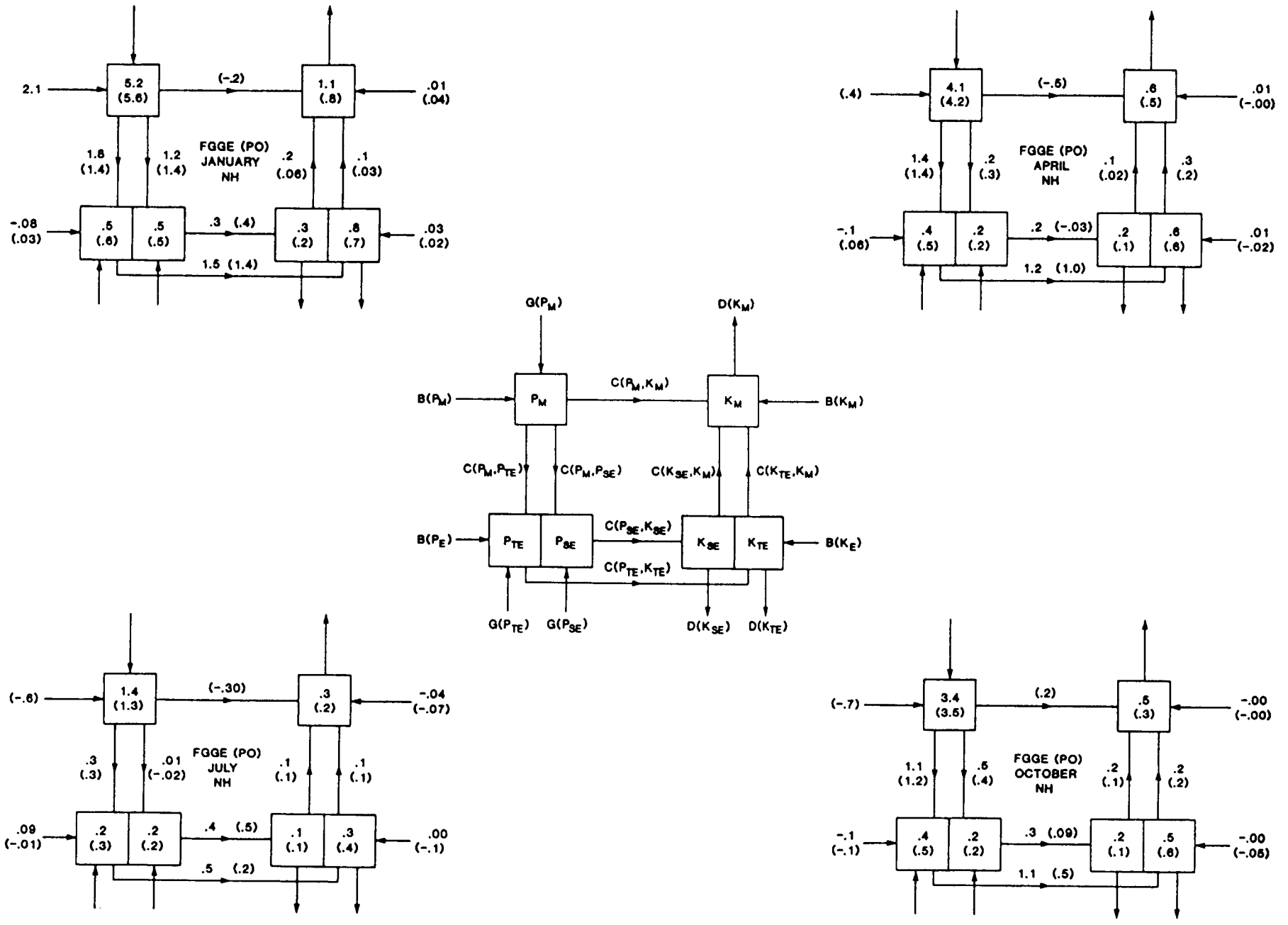

Figure 18. Box diagrams of energetics from observations for January, April, July and October in the Northern Hemisphere. Results from ECMWF GWE analyses are labelled "FGGE", those from Oort and Peixoto (1974) and Peixoto and Oort (1974) as "PO". Units are $10^6 Joule/m^2$ for energies, $Watts/m^2$ for conversions.

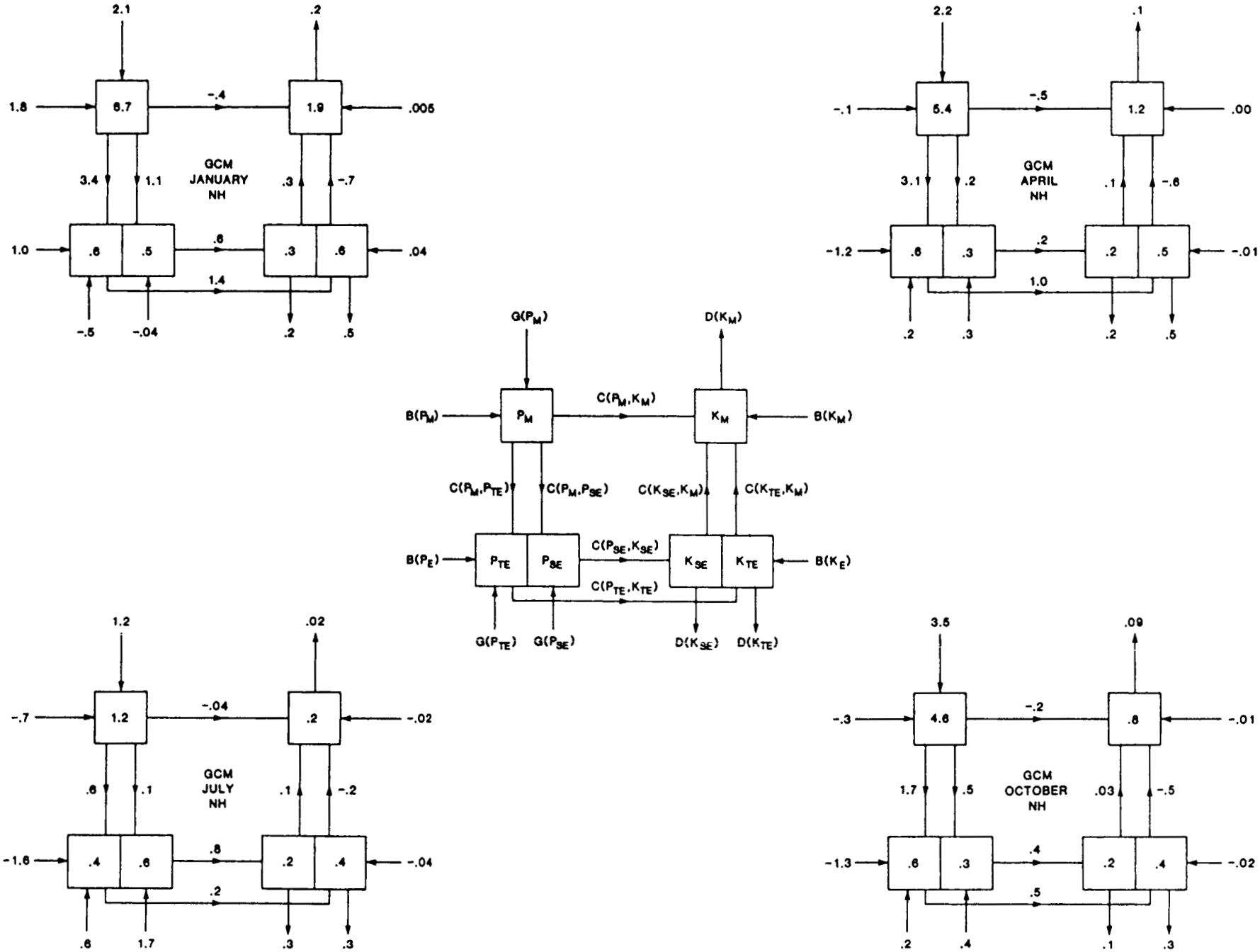

Figure 19. Box diagrams of energetics from the GCM for January, April, July and October in the Northern Hemisphere. Otherwise as in Figure 18.

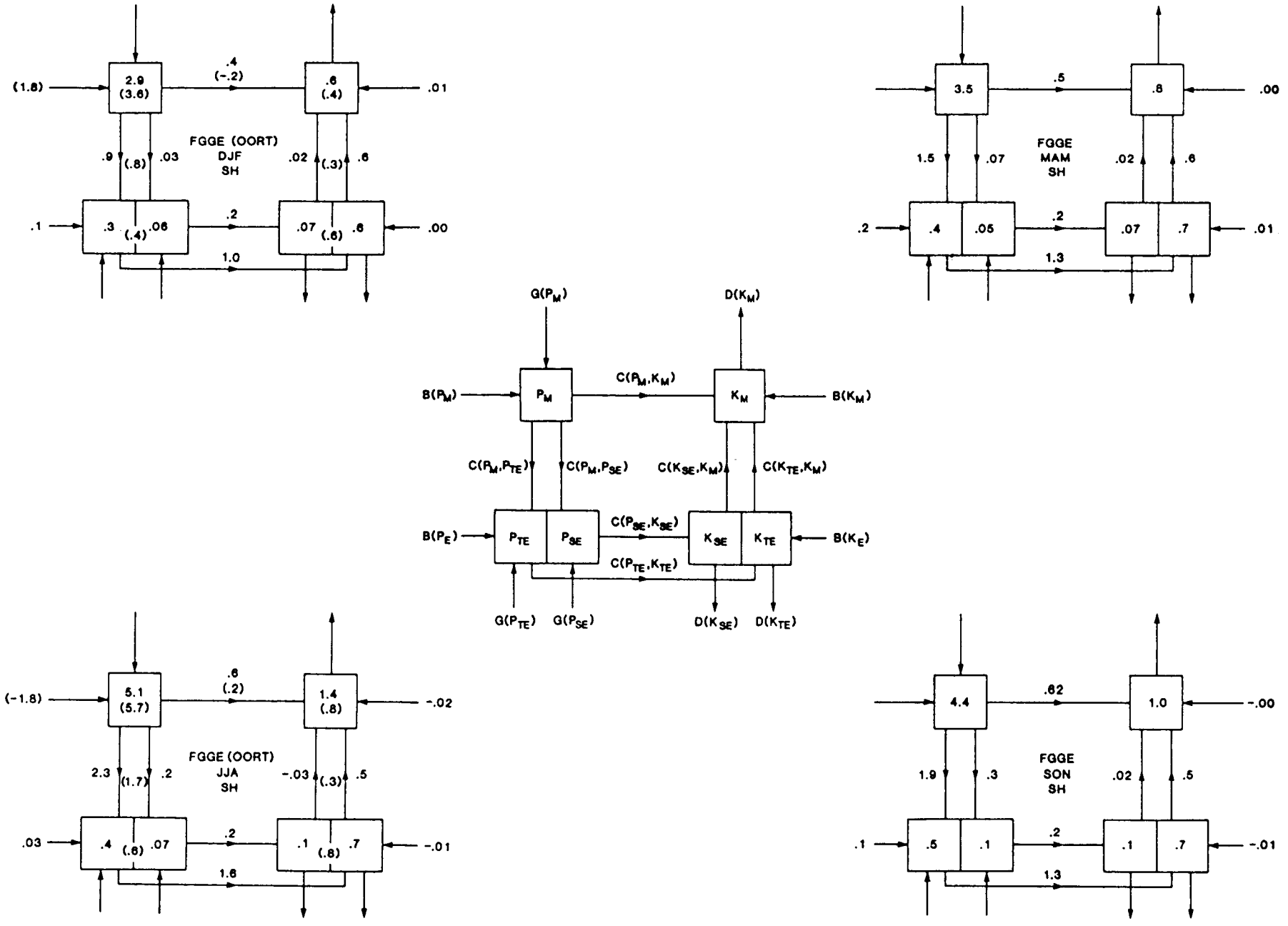

Figure 20. Box diagrams taken from observations for the four three-month seasons in the Southern Hemisphere. Otherwise as in Figure 18.

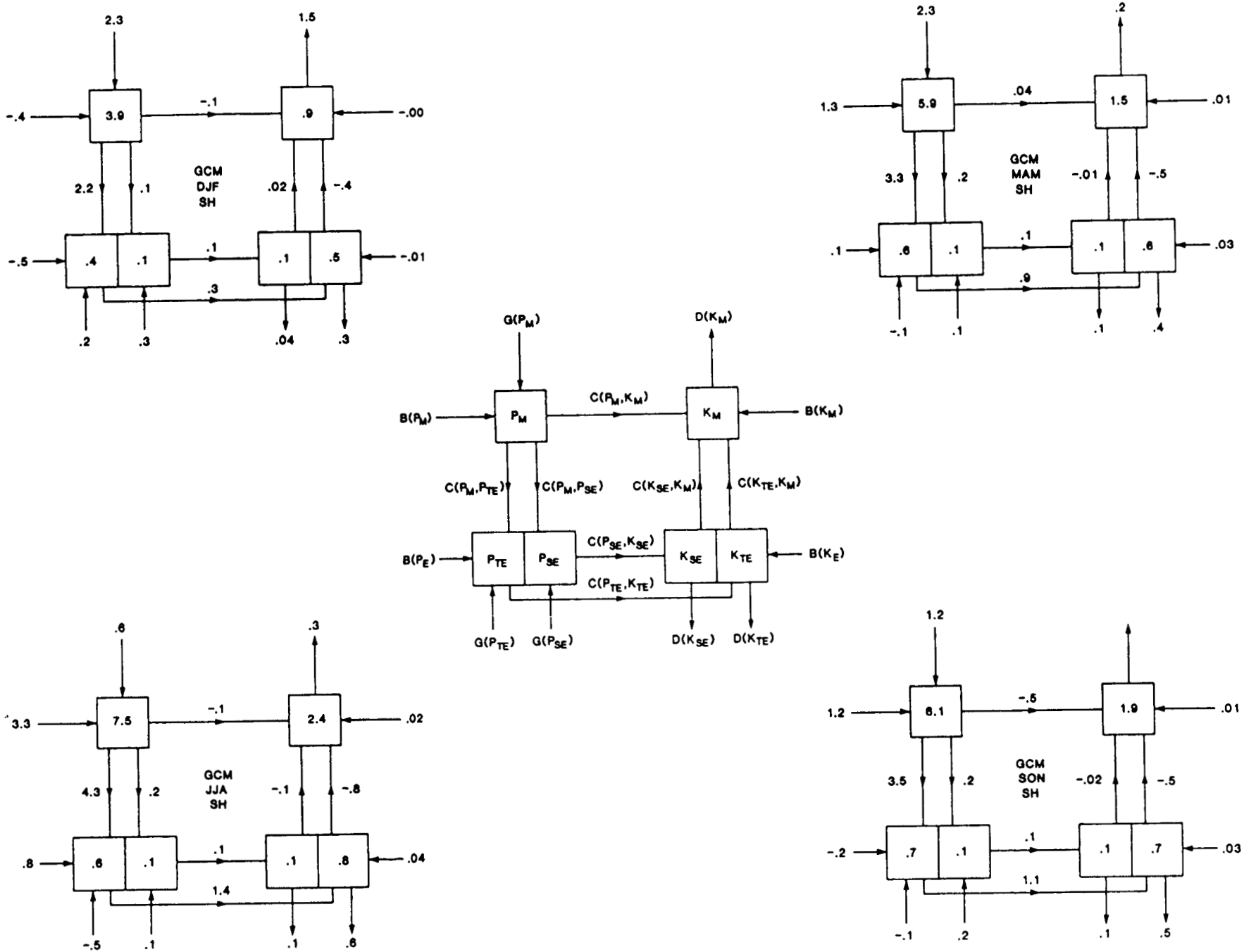

Figure 21. Box diagrams taken from the GCM for the four three-month seasons in the Southern Hemisphere. Otherwise as in Figure 18.

NASA
National Aeronautics and Space Administration

Report Documentation Page

1. Report No.	2. Government Accession No.	3. Recipient's Catalog No.
NASA TM-100714		

4. Title and Subtitle	5. Report Date
The Seasonal Cycle of Energetics from the GLAS/UMD Climate GCM	December 1988
	6. Performing Organization Code: 611.0
7. Author(s): David M. Straus and J. Shukla	8. Performing Organization Report No.: 89B00067
	10. Work Unit No.
9. Performing Organization Name and Address: Global Modeling and Simulation Branch, Laboratory for Atmospheres, Goddard Space Flight Center, Greenbelt, Maryland 20771	11. Contract or Grant No.
	13. Type of Report and Period Covered: Technical Memorandum
12. Sponsoring Agency Name and Address: National Aeronautics and Space Administration, Washington, D.C. 20546-0001	14. Sponsoring Agency Code

15. Supplementary Notes

J. Shukla - Department of Meteorology, University of Maryland, College Park, Maryland, 20742.
David M. Straus - Goddard Space Flight Center, Greenbelt, Maryland, 20771.

16. Abstract

The annual cycle of atmospheric energetics from a 2-year integration of the GLAS/UMD Climate GCM is computed and compared to results from the European Centre analyses of the GWE year, and to previously published results on a global basis. All calculations are done in the mixed space-time domain. The main conclusions are: (i) the seasonal cycle of today's eddy kinetic energy (in both hemispheres), and of the transient eddy available potential energy and the potential-to-kinetic energy conversions (mean and eddy) in the Northern Hemisphere are well simulated by the GCM; (ii) the GCM's tendency to have anomalously large mean u-winds at upper levels in high latitudes leads to excessive wintertime values of mean kinetic and available potential energies, and causes distortions in the GCM latitude-height distribution of kinetic energy and of many of the conversions; (iii) the eddy conversion of available potential-to-kinetic energy obtained from the ageostrophic wind in these analyses; and (iv) the conversions in the Southern Hemisphere are not well simulated by the GCM, although the observations are somewhat questionable.

17. Key Words (Suggested by Author(s))	18. Distribution Statement
Energetics General Circulation Models Seasonal Cycle	Unclassified - Unlimited Subject Category 47

19. Security Classif. (of this report)	20. Security Classif. (of this page)	21. No. of pages	22. Price
Unclassified	Unclassified		